Progress reports of individual researchers

Yasuo ASADA *Energy Technology*
Biocatalitic Reduction of Isooxsasoles and Hydrogen Production by Photosynthetic Microorganisms with the use of Hydrogen-Absorving Metals

Tomohiko ASAI *Nanomaterials and Nanodevices*
Control and application of self-organized magnetized plasmoid

Shigeru CHAEN and Tadashi TOJO *Nanomaterials and Nanodevices*
Imaging of Bio-molecule and Cell

Kyoko FUJIWARA, Satoru TAKAHASHI, Naoya IGARASHI, Katsumi ABE, Masayoshi SOMA *Medical* Applied chemical, physical biology: Strategy to cure cancer patients

Noboru FUKUDA, Kosuke SAITO, Jun IGARASHI *Medical*
Drug discovery of pyrrole-imidazole (PI) polyamide by the chemical biology

Hideomi HASHIBA *Quantum Information; Nanomaterials and Nanodevices*
Single Photon Optoelectronics Devices

Takuya HASHIMOTO *Energy Technology*
Preparation of Materials for Intermediate Temperature Solid Oxide Fuel Cells with Nano-mixing Process

Hiroki IKAKE *Supramolecules and Self-Assembly*
Development of Poly(lactic acid)s Films as biopolymer, and Applications to New Material Field

Shuichiro INOUE *Quantum Information*
Experimental demonstration of bosonic quantum interference of single surface plasmon-polaritons

Hiroshi ISHIDA *Quantum Theory and Computation*
Electronic Structure and Conductance of Strongly Correlated Nanosized Structures

Akiyoshi ITOH, Arata TSUKAMOTO *Information Storage; Supramolecules and Self-Assembly*
Ultra High Density Information Recording Materials on Self Assembled Nano-structured Substrates

Nobuyuki IWATA *Nanomaterials and Nanodevices*
Analysis of Crystal Structures of Antiferromagnetic Cr_2O_3 Thin Films Using Reciprocal Space Mapping

Ken JUDAI *Nanomaterials and Nanodevices*
Nano Helical Morphology of Silver Acetylide Compounds

Koichiro KANO *Medical*
The remodeling of actin stress fibers is a trigger for in vitro adipocyte differentiation

Tsugumichi KOSHINAGA, Shouta UEKUSA *Medical*
Potential of new therapeutic and diagnostic technology using PI polyamide and nanostructure in neuroblastoma

Takeshi KUWAMOTO *Quantum Information*
Experimental Studies for Quantum Memory using Neutral Atoms

Yoshikazu MASUHIRO *Medical*
Application to the iPS induced factors of DP-1 Stabilon motif inhibiting proteolysis

Yoshiaki MATSUMOTO, Takahiko AOYAMA *Medical*
Pharmacokinetic/Pharmacodynamic Analysis of Tumor-localizing Photosensitizing Compounds

Sachiko MATSUSHITA *Supramolecules and Self-Assembly ; Energy Technology*
Self-assembly and Self-organization from the viewpoint of Device-fabrication Methods

Hiroki NAGASE *Medical*
Applied chemical biology: strategy to cure cancer patients

Katsuji NAKAGAWA *Information Storage*
Research for high density and high speed magnetic recording- Thermally assisted magnetic recording applying near field optical light -

Nobuyuki NISHIMIYA *Energy Technology*
Composite Formation of Hydrogen Occlusion Alloys and Photo-Related Phenomena Thereof

Shinichiro OHNUKI *Quantum Theory and Computation*
Nano-Electromagnetic Simulation and Its Applications to Plasmonic Devices

Joe OTSUKI *Supramolecules and Self-Assembly; Energy Technology*
Self-Assembled Supramolecules and Their Applications to Energy, Medical, and Information Technologies

Tokuei SAKO *Quantum Theory and Computation*
Conjugate-Fermi-hole analysis in the origin of Hund's rule and the interaction between atoms and strong ultrashort pulsed laser lights

Kaoru SUZUKI *Nanomaterials and Nanodevices*
Synthesis of Nano-rod Devices with Wide Band Gap Semiconductor Effect

Yoshiki TAKANO *Nanomaterials and Nanodevices*
Mechanism of Superconductivity in Layered Fe-based Superconductors and Search of New Superconducting Compounds

Arata TSUKAMOTO, Akiyoshi ITOH *Information Storage; Supramolecules and Self-Assembly*
Ultra Fast Information Recording and Ultra Fast Photo Magnetic Switching

Tsuneki YAMASAKI *Quantum Theory and Computation*
Propagation Characteristics and Distribution of Energy Flow by Dielectric Waveguide with Diamond Dielectric Structure in the Middle Layer

Biocatalitic Reduction of Isooxsasoles and Hydrogen Production by Photosynthetic Microorganisms with the use of Hydrogen-Absorving Metals

Yasuo ASADA
Energy Technology Group

Biocatalitic reduction of isooxasoles and acetophenon using photosynthetic bacteria, and hydrogen production by cyanobacteria combined use of hydrogen-absorbing metals are studied.

1. Biocatalitic reduction of isooxasoles and acetophenon by photosynthetic bacteria

Biocatalitic and assymetrical reduction of isooxasoles and acetophenons by photosynthetic bacteria are studied.

Intact cells of some cyanobacteria are known to convert isooxasoles to its alcohol form. The responsible enzyme is assumed to be alcohol dehydrogenase(s), but there has been detailed information. The aim of study is to clarify the responsible enzyme and strengthen the activity by genetic engineering.

We have already acquired transconjugant photosynthetic bacterium, *Rhodobacter sphaeroides* RV with three alcohol dehydrogenase (ADH) enzyme genes from the cyanobacterium, *Synechococcus* PCC7942 and one ADH gene from alcohol-assimilating photosynthetic bacterium.

This fiscal year, we tried to analyze ADH activity by activity staining of native electrophoretic gels.

The cell-free extracts from *Rhodopeudomonas palustris* No.7 in the gels was able to oxidize S-form 1-phenyl alcohol to acetophenon but not R-form.

2. Hydrogen production by photosynthetic microorganisms with the use of hydrogen-absorbing metals

(Co-works with Prof.Nishimiya, CST, Nihon-Univ.)

The new methods to collect and stimulate hydrogen produced by cyanobacteria with the use of hydrogen-absorbing metals.

The hydrogen gas produced by cyanobacteria, *Spirulina platensis* and *Anabaena cylindrical* was collected with hydrogen-absorbing metals. By reducing hydrogen partial pressure, the hydrogen production by cyanobacteria, was stimulated. *Spirulina platensis* produces hydrogen gas by anaerobic digestion of intracellular glycogen. However, the stored hydrogen gas is inhibitory for the hydrogen production. By lowering hydrogen partial pressure with the use of hydrogen-absorbing metals, hydrogen production was stimulated.

Control and application of self-organized magnetized plasmoid

Tomohiko ASAI
Nanomaterials and Nanodevice Group

Self-organized magnetized plasmoid has attractive advantages for the variety of applications because of its wide range of plasma parameters and its ease of control. In this work, applications of the plasmoid for rapid thin-film deposition and EUV light source have been proposed and demonstrated. Also, several innovative applications of plasma formation technique have been proposed and initiated in this project.

1. Development of high-speed film deposition technique by magnetized coaxial plasma gun

Magnetized Coaxial Plasma Gun (MCPG) has been applied for new alloy film deposition technique. This method realize the generation of metallic thin film with the materials which have high-melting-point (e.g., Ti, Zr …). Generation methods for these materials had been limited to the ion beam assisted vacuum deposition. The optimization of gun design and the initial experiment with composite material electrode have been performed. In the experiments with horizontal plasmoid ejection into 500mm long drift tube, metallic thin-film was deposited on the vertically placed substrate. In this test, generated plasma has been investigated by a spectroscopic method. Successfully ionized and accelerated metallic materials have been confirmed. Now operation condition for thin film generation have been optimized.
(Collaboration with Prof. K. Suzuki and Prof. N. Nishimiya)

2. High frequency repetitive operation (10kHz) and merging of Spheromak for VUV light source

An ionized plasmoid generated by MCPG tends to be relaxed into a force-free equilibrium called "spheromak" in a conductive metallic chamber which roles as a flux conserver. Counter injection of spheromaks into the flux conserver is followed by a magnetic reconnection event which heats the plasma itself by the dissipation of magnetic energy into plasma energy. This realizes a compact high-temperature plasma source which can be applied as a EUV (Extreme Ultraviolet lithography) light source. In this year, a grazing-incidence spectrometer (Fig. 1) for the band from 5 - 30nm had been developed and the wavelength dependency of emission have been started to measure.

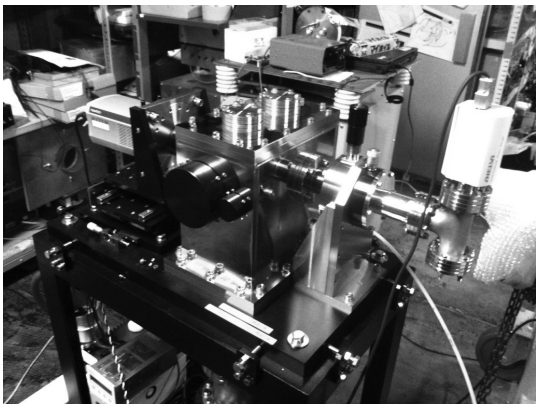

Figure 1. A grazing-incidence spectrometer for the plasmoid collision EUV light source.

3. Electrodeless plasma source using rotating magnetic field

Steadily operated plasma source using rotating magnetic field (RMF) technique has been studied aiming to the applications for a light source and a plasma treatment method. The application of magnetic circuit with high permeability material on RMF antenna has been realized higher efficiency of plasma formation. This has been applied for a patent through NUBIC (JP2011-068129).
(Collaboration with Prof. M. Inomoto, University of Tokyo)

Imaging of Bio-molecule and Cell

Shigeru CHAEN and Tadashi TOJO
Nanomaterials and Nanodevice Group

1. Studies on the biomolecular motor using the ordinary fluorescent imaging technique.

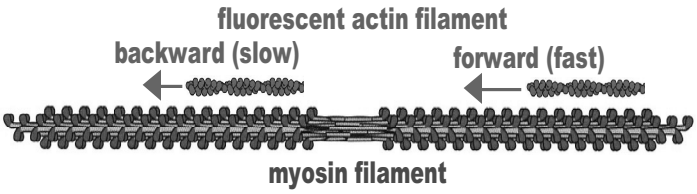

In vitro motility assays using bipolar myosin thick filaments demonstrated that actin filaments slides slower in the direction leading away from the central zone than towards it. Recently, we have suggested that the backward movement causes the myosin heads to be constrained and increase in the energy required for the ADP release step by the findings that the thermal activation energy. (Publication 1). In this study, in order to examine whether ADP release rate is slower in the backward than the forward movement, we constructed an assay system to estimate the ADP release rate from the displacement of fluorescent nucleotides bound to myosin heads by flash photolysis of caged ATP. Using the new assay system, we obtained that ADP release rate is slower in the backward than the forward movement.

2. Development of a new wet cell using a carbon thin diaphragm to observe a living cell in aqueous solution with Scanning Electron Microscopy at nanometer resolution

In electron microscopy, transparency of specimens against a beam of electrons in TEM or intensity of secondary electrons and so on induced by an incident electron beam in SEM is translated into contrast. Any material surrounding a specimen, which prevents electron beam passing or detection of secondary electrons, obstructs to create an image. Hence, electron microscopy intrinsically requires high voltage electron beam irradiation of specimens and high vacuum under 10-4 Pa in the cell for specimens. Water in samples must be replaced with some resins or completely dried up. These conditions make it difficult to observe wet or living samples like enzymes retaining catalytic activities or living cells in aqueous solution. To image wet and living samples using electron microscopy at nanometer resolution, we are developing a new wet cell for SEM whereby living cells and enzymes can be maintained in aqueous solution. A carbon thin layer with thickness of 20 nm was made by vacuum evaporation. We applied it as a diaphragm withstanding a pressure gap for separating a specimen in solution at atmospheric pressure from high vacuum environment. Cells and enzymes were placed on its surface of the atmospheric side. They were imaged using SEM. The EM photographs show detailed structures of the cell membrane and the enzymes.

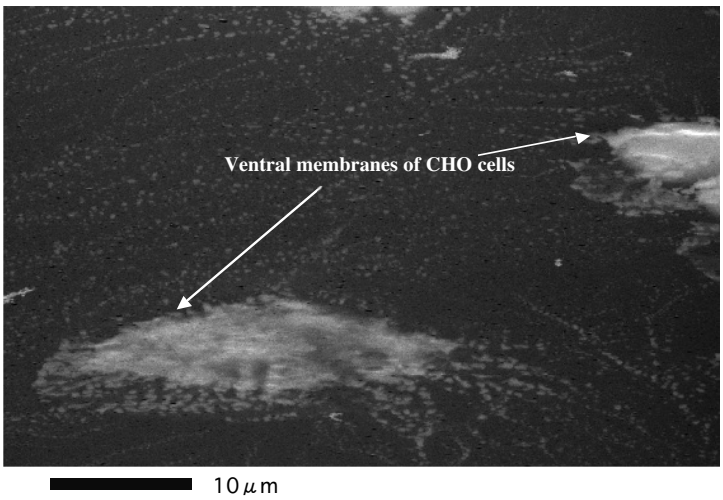

Applied chemical, physical biology: Strategy to cure cancer patients

Kyoko FUJIWARA, Satoru TAKAHASHI , Naoya IGARASHI, Katsumi ABE, Masayoshi SOMA

Medical Group

We have been conducting the projects to develop new cancer diagnostic reagents and new strategy for anti-cancer therapy based on nano-biological and chemical-biological techniques. Under the close collaboration with Professor Joe Otuski in the College of Science and Technology, we have been developing radio-sensitizer for cancer therapy.

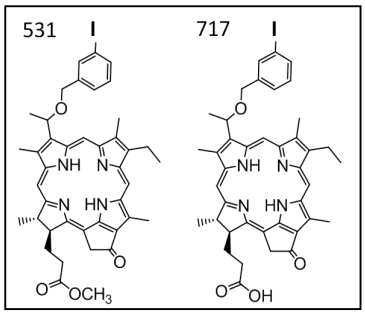

Figure1 Structure of 531 and 717
In HPPH-Gd, I of 531 is replaced with Gd.

In Photo-Dynamic Therapy (PDT), patients with tumor are treated with photo-sesitizing drugs like porphyrin derivatives systemically or locally, prior to the irradiation with laser light. Activation of the porphyrin derivetives induce photo-chemical reaction to generate reactive oxygen species (ROS), which cause cell death. Since porphyrins are taken into cells via LDL-receptor, and tumor cells expressed LDL-receptor far more than normal cells, the porphyrins could accumulate tumor tissues predominantly. Even though laser light has the merit of not harming surrounding normal tissues, however, laser at the wavelength specific for porphyrins can't reach to tumors slocated in deep under skin. That' why medical insurance cover PDT only for limited malignancies, like early lung cancer, esophagus cancer on located on surface and early cervical cancer.

We have been examining the effect of HPPH (3-(1'-hexyloxyethyl)-3-devinylpyropheophorbide-a) and its derivatives, 531, 717 and Gd-HPPH as X-ray sensitizer on many kind of tumor cell lines. HPPH has been already proven to have PDT effect. 531 is an intermediate product generated during the process to make HPPH-I[24] from HPPH, having cold iodine. Gd-HPPH has almost same structure as 531 but it contains gadolinium (Gd) instead of iodine(I). 717 is also similar to 531 but it has hydroxyl residue instead of methoxyl residue. That difference make 717 more hydrophilic than 531.

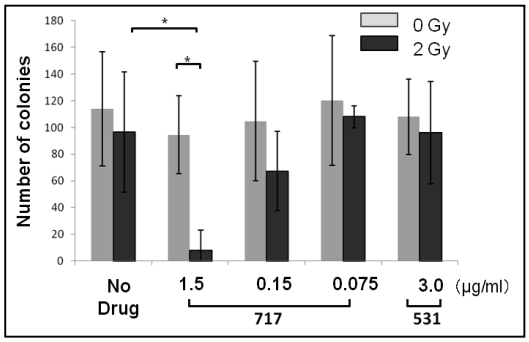

Figure2 Radio-sensitizing effect of 717
Osteosarcoma cell line MG63 was treated with 531 or 717, prior to the irradiation of 2Gy X-ray. Number of the colonies was counted 10 days after the irradiation.

Since I and Gd have a capacity to absorb X-ray, and have been used as radiocontrast agents, we expected that the HPPH derivatives with I or Gd could work as radio-sensitizer on cultured cells. We treated cell lines of human bladder cancer, breast cancer and osteosarcoma with 531, 717 and HPPH-Gd, followed by the irradiation with 2Gy X-ray, which never induce any cellular disorder in the absence of sensitizer, then we found that only the cells treated with 717 prior to irradiation died. The cells seemed to die in apoptotic manner. 531 and HPPH-Gd did not affect cell viability. That result indicated that I and Gd are not essential for the radio-sensitizing effect of HPPHs. We analyze the intracellular localization of HPPH derivatives by examining cell fraction with HPLC, and proved that those compound accumulate in mitochondria and golgi body rather than nuclear and cytoplasm.

It is widely believed that X-ray induce ROS by interacting with H_2O molecules, and that cause DNA double strand break and result in cell death. There is no proper explanation of how 717 distributing outside of nuclei could induce cell death, yet. We are now trying to elucidate whether 717 treatment prior to irradiation could induce ROS, and could increase the frequency of DNA break.

Drug discovery of pyrrole-imidazole (PI) polyamide by the chemical biology

Noboru FUKUDA, Kousuke SAITO, Jun IGARASHI
Medical Group

To develop DNA-recognized novel small molecule PI polyamide targeting human TGF-β1 as practical medicines, we tried to determine a lead compound, and provide the preclinical studies using common marmosets. We also develop the Nihon University original methodology to induce iPS cells using the PI polyamide targeting human TGF-β1.

I. Determination of a lead compound targeting human TGF-β1

Among seven PI polyamides designed to bind on the promoter region of human TGF-β1 gene, we selected GB1101, GB1105, and GB1106, and examined their effects on expression of TGF-β1 mRNA in humen cultured vascular smooth muscles. GB1105 and GB1106 strongly inhibited expression of TGF-β1 mRNA in a dose-dependent manner. Effect of GB1105 was strongest to inhibit the expression of TGF-β1 mRNA in human cultured fibroblast.

II. Establishment of ointment containing PI polyamide targeting human TGF-β1

We start to establish ointment containing PI polyamide targeting human TGF-β1 to develop PI polyamide as a practical medicine for the skin hypertrophic scar collonborating with solution manufacturing room in Nihon University Itabashi Hospital. We checked the combination of components of soluble materials and solutions for PI polyamides.

III. Preclinical study for PI polyamides using common marmosets

The preclical study using the primates is essential to develop PI polyamides. We chose common marmosets that are compact and have a reproductive power for the preclinical study.

1. We made contract with Central Institute for Experimental Animals as prace for the practical experiments.
2. We confirmed homology and the binding site of PI polyamides targeting human TGF-β1 on the promoter resion of marmoset TGF-β1 gene.
3. Effects of PI polyamides targeting human TGF-β1 in fibroblasts from common marmosets

We confirmed the inhibitory effects of PI polyamides targeting human TGF-β1on expression of TGF-β1 mRNA with angiotensin II.

IV. Development of the Nihon University original methodology to induce iPS cells using the PI polyamide targeting human TGF-β1

1. We evaluated efficiency to induce iPS cells with the iniciation factor, TGF-β1 inhibitor, PI polyamide targeting human TGF-β1, Apigenin, TGF-β1antagonist and Apigenin, and TGF-β1 and PI polyamide targeting human TGF-β1.
2. In addition, we combined the technologies to easily deliver the plasmides coding MTM, inducing the cell membrane permeability activity, and Stabilon that induce stabiliy of proteins.

Single Photon Optoelectronics Devices

Hideomi HASHIBA
Nanomaterials and Nanodevices Group; Quantum Information Group

Our research aims development of single photon optoelectronic devices. Our research has focused on silicone waveguides for quantum information transport, two dimensional TiO_2 photonic crystals of low refractive index for solar cells, and single photon detectors for THz range this year.

1. Development of fabrication technology of silicone waveguides with ICP etching

Semiconductor wave guides and photonic crystals are increasingly important in optoelectronic devices for quantum information technology. We study silicone wave guide devices with its third-order nonlinearities. Research of silicone wave guide devices of this year has been focused on development of simple fabrication method of the waveguides with ICP plasma etching with CF_4 gas on SOI. CF_4 plasma at high pressure and low power on ICP shows suitable etching ratio and small roughness of side-walls of less than 20 nm to few hundred nano-meter wide Si patterns covered by metal-masks.

2. Two dimensional TiO_2 photonic crystal as photo sensitized solar cell

Our two dimensional phonic crystals (PCs) of titanium oxide (TiO_2) of low refractive index to meet the needs of the advanced solar cells are fabricated with standard electron beam resist mask and sputter deposition techniques. The patterned TiO_2 layer is rutile, and it need to be anatase to be catalyst of dye sensitized solar cells. We studied required temperature and condition of the TiO_2 layers to turn into anatase. Observation of the layer baked at 250 degrees baking under XRD measurement shows that some rutile turns into anatase at that temperature.

3. THz plasma excitations of quantum dots confined with shallow potential barriers

We studied the "Single-electron transistors in THz range". THz range single photon detectors are assembled from a GaAs/AlGaAs quantum dot coupled with a metallic single electron transistor which senses appearance of charge state of the QD. Plasma excitations of the QD arises with a formation of confinement potential barrier from the reservoir having resistances more than resistance quanta, and we revealed that appropriate shape of the barriers lowers dark counts by suppression of flow of hot electrons form the reservoir. We also show that the QD works as a heat bath from THz plasma excitations. This will promise high temperature operation of the THz detection.

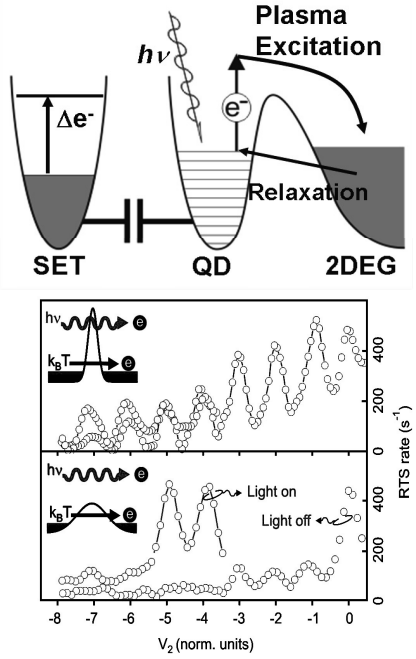

Preparation of Materials for Intermediate Temperature Solid Oxide Fuel Cells with Nano-mixing Process

Takuya HASHIMOTO
Energy Technology Group

Solid oxide fuel cell (SOFC) attracts much interest as energy conversion device with high energy efficiency and low cost owing to high operating temperature and no necessity of Pt catalyst in electrode. However, instability during long period and a few alternatives for materials due to too high operating temperatures are problems for application. Decrease of operating temperature as low as about 600 ºC would solve the problems. The purpose of this study is development of new electrolyte and electrode materials which are inevitable for low temperature operation of SOFC. In particular, using liquid phase process by which mixing with nano-scale is probable, challenged is preparation of high functional new materials whose preparation have been difficult or mechanical strength and density is low with conventional solid state reaction process. From this year, sintering temperature dependence of pore size with several tens nm~ several hundreds nm and its distribution in the electrode materials have also been investigated.

In this year, following three themes have been performed.

1. Preparation of new proton conductor, $Sr_{1-x}Ba_xZr_{1-y}Y_yO_3$ with liquid phase mixing method and evaluation its proton conductivity.
2. Preparation of new cathode material, $LaNi_{1-x}Fe_xO_3$ and control of its pore size and distribution.
3. Preparation of new anode material, $Sr_{2-x}La_xFeWO_6$ and evaluation of its stability.

In this presentation, results of the second theme are presented.

For materials of cathode of SOFC, not only high electrical conductivity and stability at high temperatures but also moderate porosity to enable introduction of O_2 gas near electrolyte are required. So far, we have proposed that $LaNi_{0.6}Fe_{0.4}O_3$ is promising as cathode material because of high conductivity at high temperature, high stability due to no Sr and similar thermal expansion coefficient to those of electrolyte materials. However, no study has been carried out that sintering density, specific area, pore size and its distribution, which are important for application, can be controlled. In this study, sintering property of pressed pellet of $LaNi_{0.6}Fe_{0.4}O_3$ powder, prepared with Pechini method, has been investigated with not only measurement of density but also measurements of specific area and pore size and distribution using N_2 adsorption.

The porosities of the specimens sintered at 1000 °C and 1100°C were 38 % and 28%, respectively. Since 30 % porosity is reported to be desirable for cathode materials, it can be proposed that sintering at around 1050 °C is appropriate. Figure 1 shows pore size distribution of $LaNi_{0.6}Fe_{0.4}O_3$ ceramics sintered at 900-1200 °C. Two peaks were observed around 250 nm and 2 nm. Pore around 250 nm enables to introduce O_2 gas near electrolyte. Although the volume of the pores decreased with increasing sintering temperature, the peak around 250 nm remained even at sintering temperature as high as 1100 °C. Therefore, it can be concluded that $LaNi_{0.6}Fe_{0.4}O_3$ ceramics sintered at 1050 °C has pores through which O_2 gas can diffuse to the surface of the electrolyte.

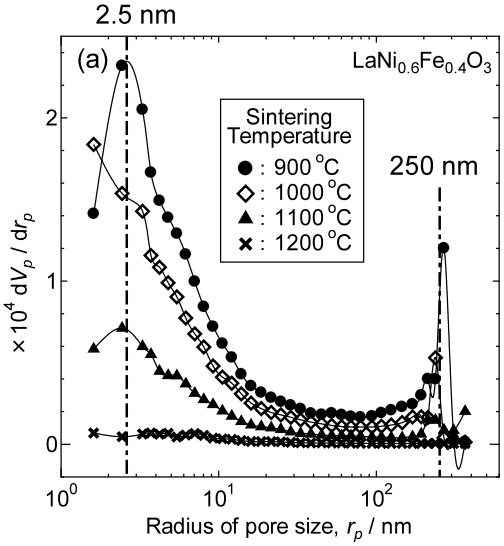

Fig. 1 Pore size distribution of $LaNi_{0.6}Fe_{0.4}O_3$ ceramics sintered at 900-1200 °C.

Development of Poly(lactic acid)s Films as biopolymer, and Applications to New Material Field

Hiroki IKAKE
Supramolecular and Self-Assembly Group

In our group, the aim of development of poly(lactic acid) (PLA) films as biopolymer with the high thermal- and mechanical- resistance. And then, the improved PLA was submitted to new material field.

1. Development of Poly(lactic acid) Films with Exhibiting the Piezoelectricity

It is well known that poly(L-lactid) (PLLA) fibers exhibit the piezoelectricity, in which their piezoelectric constant increases with increasing degree of crystallinity and uniformity of the orientation of the crystallites. Recently, bending motion due to their piezoelectricity has been reported (Fig.1). The *zigzag* motion is closely related to the morphology of PLLA fibers. For this purpose, the irradiated magnetic field, and other process, under the electric field, have produced the high oriented PLLA films. In the present study, we successfully synthesized PLLA using condensation polymerization, and the crystallites of PLLA became the growth by the heat treatment.

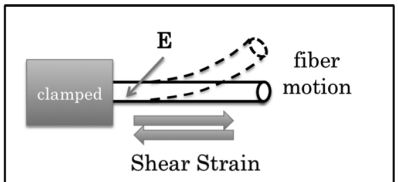

Fig.1 The piezoelectric motion of polymer fiber*.
* M. Honda, K. Hayashi, K. Morii, S. Kawai, Y. Morimoto, and Y. Tajitsu, *Jpn. J. Appl. Phys.*, 46, 7122-7124 (2007).

2. Preparation of High Crystallinity and High Orientation Poly(L-lactic acid) Films under Electric Field

Semi-crystallized PLLA has a comparatively low-degree of crystallization (X_c). In order to orient its crystalline domains in a regular way and to raise X_c, electric field was applied to PLLA film while annealing it according to a program. As a result of the analysis by wide-angle X-ray diffraction (Fig.2), it was shown that the crystalline domains have a tendency to orient in parallel to the direction of the applied electric field and the orientation is best regulated at annealing temperature of 170°C. Analysis of X_c and the crystalline lamella by differential scanning calorimeter and small-angle X-ray scattering has suggested that such a regulated orientation of the crystalline domains might be brought about by small crystalline of sub-micron order, produced at the annealing temperature of 170°C.

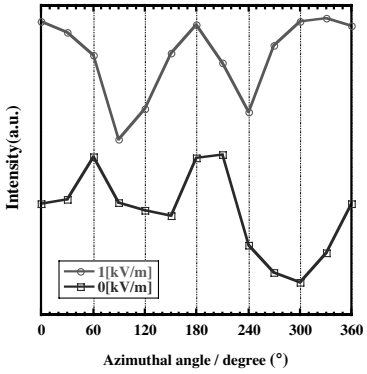

Fig.2 WAXD(110)/(200) intensity along the azimuthal angle for PLLA films.

3. Morphological change of Poly(L-lactic acid) Films with Magnetic Irradiation

In this study, we discussed that influence of morphological change of PLLA films on magnetic irradiation. Annealing process for PLLA films was the same as in the electric field's program. As a result of the analysis by wide-angle X-ray diffraction, it was shown that the crystalline domains have a tendency to orient in parallel to the direction of the applied magnetic filed and the orientation is best regulated at annealing temperature of 170°C. Fig.3 showed that the small-angle X-ray scattering (SAXS) profiles of heat-treated PLLA films. Analysis of the crystalline lamella by SAXS has suggested that such a regulated orientation of the crystalline domains might be brought about by small crystalline of sub-micron order, produced at the annealing temperature of 170°C.

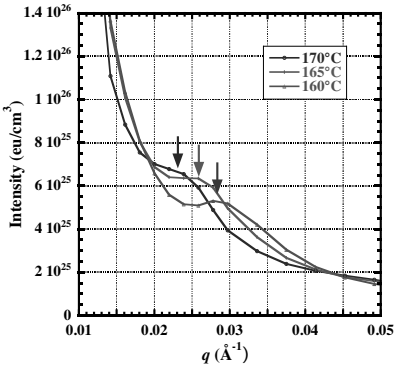

Fig.3 SAXS profiles of PLLA films treated at 160°C, 165°C and 170°C.

Experimental demonstration of bosonic quantum interference of single surface plasmon-polaritons

Shuichiro INOUE
Quantum Information Group

Recently, surface plasmon polaritons (SPPs) have attracted much interest in the research area of quantum information technologies because of their importance for an enhanced nonlinear process and an efficient coupling with nanoscale electronic systems. In order to realize the quantum information processing with the SPPs, the quantum nature of single SPPs must be investigated. In this work, we experimentally demonstrated the quantum interference of single SPPs using a 50/50 directional coupler and superconducting photon number resolving detectors.

1. 50/50 directional coupler (DC) based on long-range SPP waveguides

The DCs we fabricated were composed of long-range SPP (LR-SPP) straight waveguides and S-bends. (Fig.1) Our LR-SPP waveguides consist of a thin gold stripe (thickness of 20 nm, width of 8 μm) embedded in a UV-curable acrylate (ZPU-12-450) for upper and lower cladding layers of 22 μm. The efficient coupling and the LR-SPP mode excitation were achieved by the butt-coupled connection between an optical fiber and the DC. To connect optical fibers to all input and output ports of the DC, the each port was separated by 200 mm. In order to realize the output ratio of 50/50, we have chosen an interaction length of 500 mm and a separation distance between the coupled waveguides of 0 mm. The insertion loss of the DC was approximately 30 dB.

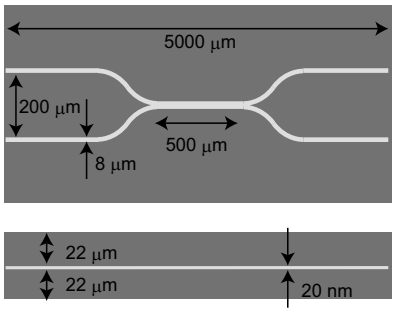

Fig. 1 Au nano-stripe DC

2. Generation of single SPPs and bosonic quantum interference

Our experimental setup is schematically depicted in Fig. 2. A photon pair at 1551 nm (signal- and idler-photons) is generated through a spontaneous parametric down conversion process in a type-II periodically poled lithium niobate (PPLN) pumped by a CW-laser at 775.5 nm. The signal- and idler-photons coupled to the DC excited the single SPPs. The interfered single SPPs were converted into photons at the end of the DC, and they were detected by the photon-number resolving detectors based on titanium superconducting transition edge sensors (PNRD1, 2). The detection efficiency, the photon-number resolution and the dark count rate of the PNRDs were 84 %, 0.29 eV and 10 Hz, respectively. Fig. 3 shows the measured coincidence counts between 2-photon detection in the PNRD1 and 0-photon detection in the PNRD2 as a function of the optical path difference. At a certain optical path difference, coincidence counts increased. This means that the quantum interference of the single SPPs output two photons in one port or the other, which is the evidence that the single SPP is a bosonic quantum particle.

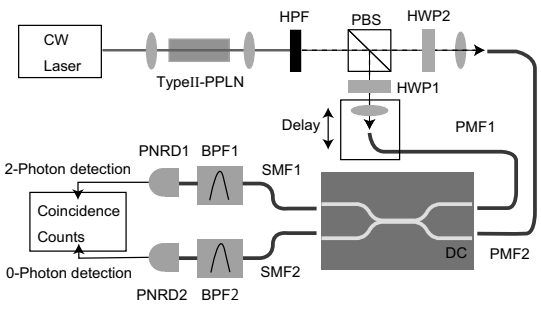

Fig 2. Experimental setup

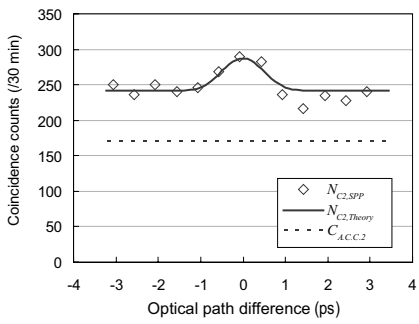

Fig 3. Quantum interference of single SPPs

Electronic Structure and Conductance of Strongly Correlated Nanosized Structures

Hiroshi ISHIDA
Quantum Theory and Computation Group

Recent progress in microfabrication technology has enabled the synthesis of nanosized structures such as single molecules suspended between metal electrodes and heterointerfaces made out of ultrathin layers of transition-metal oxides. The electronic properties of these systems are very often studied within one-electron approximation, for example, by using density functional theory. In the present work, we adopt many-body techniques such as dynamical mean-field theory to investigate the effects of strong Coulomb correlations on the electronic properties of these materials.

1. Transport properties of the Mott insulating layer adsorbed on a metal substrate

The electronic properties of the Mott insulating monolayer adsorbed on a semi-infinite metal substrate were studied by using a cluster extension of dynamical mean-field theory. In doing so, the overlayer forming a square lattice was divided into an array of 2x2 clusters, and the short-range Coulomb correlations within the cluster were fully taken into consideration. We calculated the in-plane and out-of-plane components of the conductance of the overlayer by using the Kubo formula. While the Mott insulating layer becomes metallic when it is coupled with a substrate metal, the (p,0) component of the electron self-energy induced by short-range electron correlations exhibits a finite scattering rate. Moreover, this scattering rate is found to increase with decreasing temperature, which results in an increase in the in-plane electrical resistivity of the overlayer with decreasing temperature (publication 1).

2. Conductance of strongly correlated atomic chains between two metal electrodes

We have studied the electron conductance of monoatomic chains suspended between two metal electrodes by considering the on-site Coulomb repulsion energy in the atomic chain. As shown in Figure 1, the atomic chain is modeled by a Hubbard-type Hamiltonian consisting of N atoms, while the semi-infinite metal electrodes on both sides are represented by a non-interacting tight-binding model. For simplicity, we considered the small bias voltage limit and calculated the equilibrium Green's function of the system at a finite temperature. Figure 2 shows the calculated conductance s (in unit of $s_0=2e^2/h$) of the 3-atom chain as a function of the chemical potential m of the electrode (m=0 corresponds to half-filling). The non-interacting chain with U=0 exhibits three peaks in s corresponding to three molecular levels formed in the chain. With increasing U, these peaks split and are pushed toward the energy regions of the upper and lower satellite bands, while, in the quasi-energy gap region around m=0, s becomes much smaller than that of the non-interacting chain.

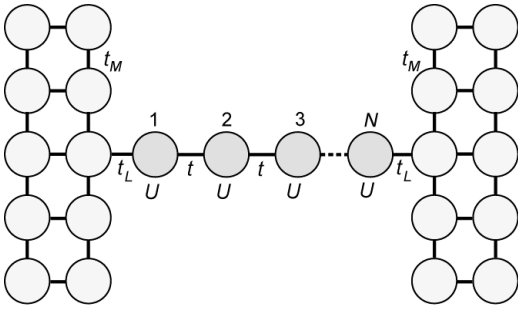

図1：金属電極間の原子架橋

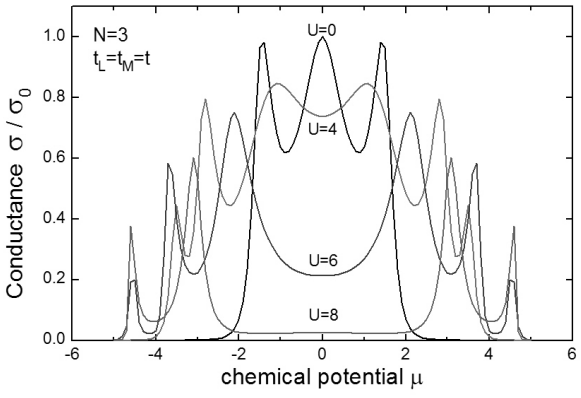

図2： 原子架橋(N=3)の電気伝導率

Ultra High Density Information Recording Materials on Self Assembled Nano-structured Substrates

Akiyoshi ITOH, Arata TSUKAMOTO
Information Storage Group and Supramolecules and Self-Assembly Group

In recent years, much attention has been focused on nano-structured magnetic media for achieving ultra high density recording up to several Tbit/inch^2. Combining self-assembly nano-structured substrates with defined magnetic properties provided by a magnetic film deposited onto the surface, enable a noble approach to create magnetic nanostructure arrays. We tried to prepare and utilize nano-structured substrates such as silica thin film having self-assembled nano-pores and self-assembled silica particle substrate.

1. A role of rapid thermal annealing (RTA) for achieving fine isolated grains

We already reported that the rapid thermal annealing (RTA) of Fe/Pt and Fe/Cu/Pt multilayered continuous films are effective to obtain perpendicularly magnetized small $L1_0$ structured grains on thermally oxidized Si substrate, and also the SiO_2 substrates having self-organized nano-pores is able to increase the grain density significantly. However, relations between the process for forming isolated grains from the continuous film and the annealing temperature are not clarified. Then, we focused onto observation of grain formation process. We fabricate FeCuPt by RTA, under the variety of heating up rate (T_R) and the maximum temperature (T_m). Isolated grains are obtained at higher T_R and T_m, however at higher T_m than approximately 550 ℃, large grains have been appeared. We introduce a rapid cooling process into RTA and comparing the results with the both cases of rapid and slow cooling processes to clarify at what temperature the isolation of grains has been occurred. With the rapid cooling process, growing of grains are prevented, however a new peaks in XRD (X-ray diffractometer) profile which correspond to the disordered structure of FeCuPt are appeared as shown in Fig. 1. (Publication 9)

2. TAMR (Thermally Assisted Magnetic Recording) simulation of FePt isolated grain by near field optical head

We performed three dimensional micromagnetic simulations of FePt isolated grains with time evolution of temperature distribution in media, for estimating recording process in TAMR with near field optical head. Three dimensional micromagnetic simulations were performed with Landau-Lifshitz-Gilbert equation. The thermal distribution in the media was determined by solving the heat equation with heat source from near field optical head. After heating of 1 ns, the temperature of heated FePt grain reached 770 K. Once the magnetization was completely demagnetized at t = 1.0 ns, then magnetization was recovered to opposite direction with time constant of around 260 ps. From Fig. 2, we could verify the magnetization of one FePt grain was reversed and the capability of one bit recording of FePt grain media by near field optical head.

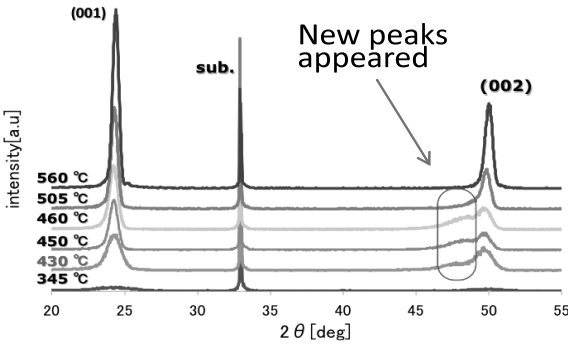

Fig. 1 XRD profile for FeCuPt annealed by RTA with rapid cooling process as a function of maximum temperature T_m for T_R 150 °C/s.

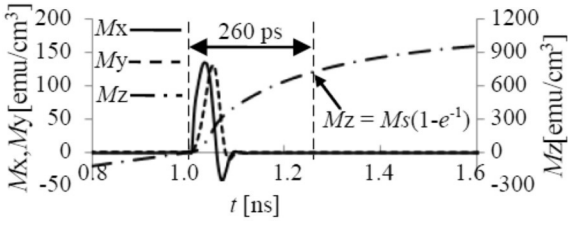

Fig. 2 Time evolution of magnetization

Analysis of Crystal Structures of Antiferromagnetic Cr_2O_3 Thin Films Using Reciprocal Space Mapping

Nobuyuki IWATA
Nanomaterials and Nanodevices Group

The crystal structure of *c*-oriented Cr_2O_3 (*c*-Cr_2O_3) and *r*-oriented Cr_2O_3 (*r*- Cr_2O_3) thin films grown on sapphire substrates was investigated in detail by two-dimensional reciprocal space mapping (RSM) using x-ray. The RSM was illustrated by detecting the diffraction signals for 10 seconds scanning ω every 0.05 degrees at fixed approximately 8 degrees wide in 2θ using one dimensional detecter, VÅNTEC-1 equipment (Bruker, D8 Discover). The angle of ϕ was adjusted to that where in-plane information can be obtained. In Fig.1, a schematic view of a corudum strcture with space symmetry of rhombohedral, $R\bar{3}c$, to which sapphire and Cr_2O_3 belong, is illustrated. In the *c*-Cr_2O_3 thin film, the RSM around $\{10\bar{1}10\}$ plane was investigated every 60 degrees in ϕ. In the *r*-Cr_2O_3 thin film, the RSMs around $\{2\bar{2}010\}$ and $\{20\bar{2}8\}$ planes were investigated. Since the corundum structure has 3-fold rotation axis along the [001] direction, corresponding planes are discribed as shown in Table I. The other planes looks like same but totally different, we call it twin, as discribed in Table I as well.

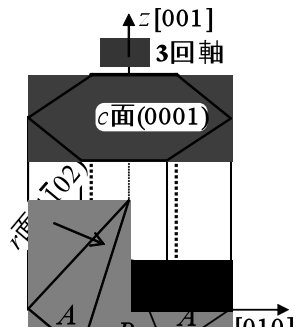

Fig.1 : Schematic structure of corundum sapphire and Cr_2O_3. *c*-plane (0001), *r*-plane ($1\bar{1}02$), and lattice plane, indicated by "*A*" and "*B*". Since there is a 3-fold axis along the [001] direction, the corresponding planes to *A*" and "*B*" are obtained to rotate every 120 degrees along the [001] axis.

Table I, Investigated planes for crystal growth analysis of *c*-Cr_2O_3 and *r*-Cr_2O_3 thin films.

Group	Planes notation	Corresponding planes	Twin planes
B	$\{10\bar{1}10\}$	$(10\bar{1}10)$, $(\bar{1}1010)$, $(0\bar{1}110)$	$(1\bar{1}010)$, $(01\bar{1}10)$, $(\bar{1}0110)$
A	$\{2\bar{2}010\}$	$(2\bar{2}010)$, $(02\bar{2}10)$, $(\bar{2}0210)$	$(\bar{2}2010)$, $(0\bar{2}210)$, $(20\bar{2}10)$
B	$\{20\bar{2}8\}$	$(20\bar{2}8)$, $(\bar{2}208)$, $(0\bar{2}28)$	$(2\bar{2}08)$, $(02\bar{2}8)$, $(\bar{2}028)$

Results & Discussion

In the results of the RSM around $\{10\bar{1}10\}$ of *c*-Cr_2O_3, the Bragg diffraction of sapphire substrate and Cr_2O_3 film appeared every 120 degrees and 60 degrees in ϕ, indicating that the *c*-Cr_2O_3 grew with twin. In the case of *r*-Cr_2O_3, the Bragg diffraction concerning about the corresponding plane of $(2\bar{2}010)$ was obtained in both of film and substrate. However, the $(20\bar{2}8)$ was not appeared. From the results of the RSM of *r*-Cr_2O_3, the film grew without twin, different to that of *c*-Cr_2O_3.

In general, the surface energy of a bulk Cr_2O_3 single crystal shows lowest *r*-plane and highest *c*-plane, and middle *a*-plane. Considering the surface energy, film surface of *r*-Cr_2O_3 should be smooth, and surface of the *c*-Cr_2O_3 should be rough. However, the results was totally oppoiste. Because of the triangle arrangement of atoms in *c*-plane, it is expected that the *c*-Cr_2O_3 easily grow with twin to reduce the strain energy due to the lattice mismatch, rahter high 4%. However, the circumstance is diffarent to that of *r*-Cr_2O_3, because the lattice structure of the *r*-plane is rectangle. From the reasons mentioned above, the *r*-Cr_2O_3 grew without twin and showed rough surface as a result.

From the view of application, it is pretty good not to have twin structure in the *r*-Cr_2O_3, because an opposite magnetoelectric signal is induced from the twin.

Nano Helical Morphology of Silver Acetylide Compounds

Ken JUDAI
Nanomaterials and Nanodevices Group

Several bio molecules self-assemble into helical structures, for example, a double helix of DNA, an a-helix of protein morphology, and so on. From the viewpoint of chemistry, helical structures have been synthesized with amphiphilic polymers as supramolecular materials. In principle, the helical structures are chiral, and the right-handed or the left-handed amphiphilic helical polymers can be controlled by the functional group of organic molecular chirality. We are attempting to prepare a chiral helix by self-assembling of achiral molecules. The aim of this work is to uncover the driving force for helical self-assembly, origin of chirality. It results in supplying basis strategy for nano architecture.

Silver *p*-tolylacetylide is a structure with substituent of a toluene molecule for a silver acetylide, and it is an achiral compound having a mirror plane originally. We have succeeded in recrystallization of this compound through a soluble intermediate of a phosphine complex. A scanning electron microscopic (SEM) image is shown below for the condition of recrystallization in ethanol solvent. Nano crystals shaped with twisted ribbons were observed. The twisted ribbons are a kind of helical structures, and the chiral helices were produced from the achiral molecules. When the solvent for recrystallization was changed to a lower polarity molecule, 2-propanol, nano crystals shaped with ribbons were not twisted contrastingly. This indicates that nano morphology between helix and non-helix can be controlled with solvents of recrystallization. The mechanism for crystal growth self-assembling helices will be examined from the point of solvent effects.

First of all, how the acetylide molecules are packed into the crystal should be clarified to measure x-ray diffraction patterns. We have been already starting to do that. However, we can right now propose one model hypothesis for the mechanism of nano helical crystal growth. The qualities of the crystals depended upon the solvent molecules of recrystallization. Many branching structures could be found in the helices recrystallized in ethanol, and contrastingly longer straight crystals were observed in the sample recrystallized in 2-propanol. It looks that lower crystal quality is associated with helical structures. An actual mechanism for the helix is unknown. As a hypothesis, lower quality of crystal growth may produce lots of defect on surface. The surface defects may generate surface tension for helical deformation.

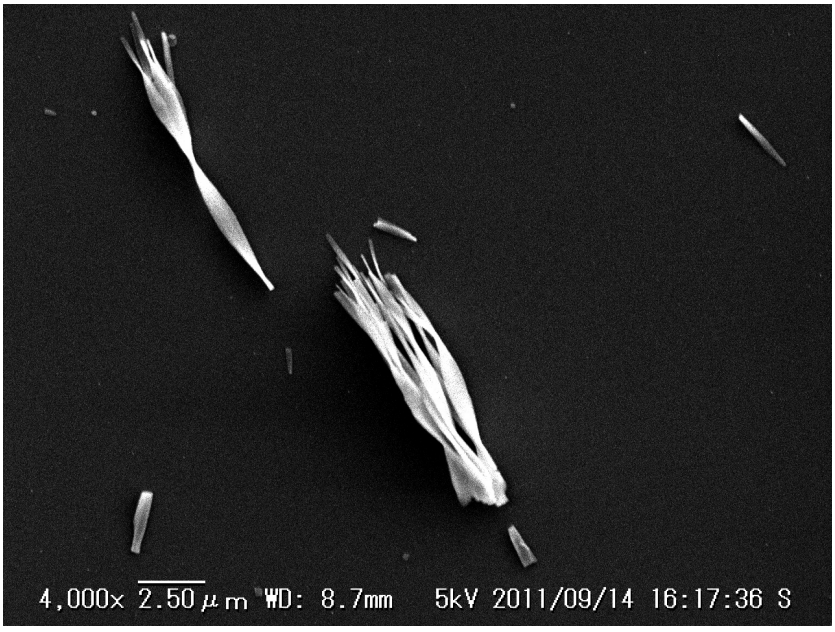

We are studying copper acetylide compounds as well as silver acetylide. The surface active copper nano particles can be prepared from copper acetylide, and catalytic activity has been investigated. Those results have been already reported in an international journal (publication 1).

The remodeling of actin stress fibers is a trigger for in vitro adipocyte differentiation

Koichiro KANO
Medical Group

Adipocyte differentiation at an early stage is directly regulated by gene expression of a master regulator such as peroxisome proliferator-activated receptor-γ (PPARγ). During adipogenesis, the remodeling of actin cytoskelton defines important events of the differentiation process. Here, we examined the regulatory relationship between actin cytoskelton remodeling and PPARγ in early adipocyte differentiation. Depending on adipogenic induction, actin stress fibers were immediately disrupted prior to the expression of PPARγ. And treatment with cytoskeletal fixation agent phalloidin maintained actin fiber structures even after adipogenic induction, and caused a down-regulation of PPARγ. In addition, ectopic expression of activated RhoA, which is known to promote the formation of actin stress fibers, inhibited the disruption of actin stress fibers and PPARγ expression after adipogenic induction, and these effects were recovered by treatment with the RhoA kinase inhibitor Y-27632. Moreover, treatment of the actin polymerization inhibitor cytochalasin D in active RhoA-expressing cells caused the disruption of actin stress fibers, and as a result, PPARγ expression was rescued. On the other hand, introduction of the PPARγ-specific shRNA resulted in maintained the high-level expression of fibronectin (FN) matrix and inhibited the reorganization into adipocyte-specific cortical actin structures during adipocyte differentiation. And transfection of FN-specific siRNA in PPARγ-knockdown cells after adipogenic induction caused the formation of cortical actin structures. In conclusion, our findings indicate that actin stress fiber disruption directly induces PPARγ expression, and that PPARγ regulates the reorganization into adipocyte-specific cortical actin structures through the down-regulation of FN matrix, and provide a novel insight into the mutual regulatory mechanisms between actin cytoskelton remodeling and adipogenic transcription factors in early adipocyte differentiation.

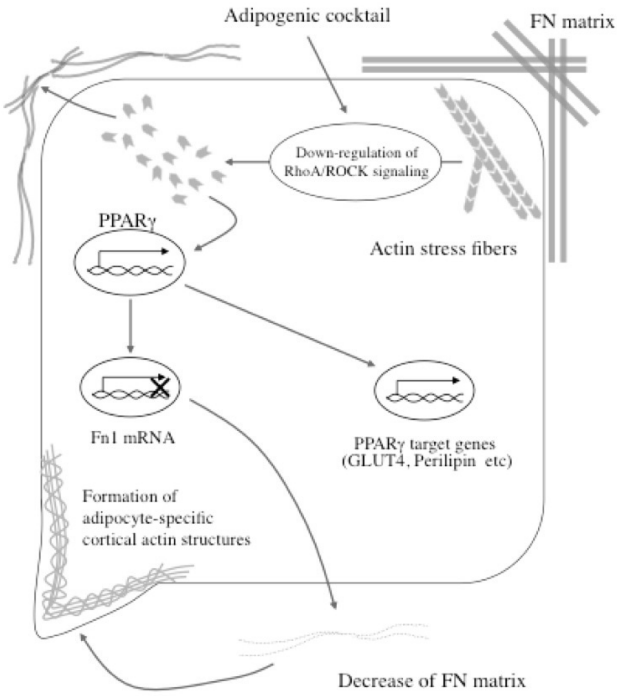

Potential of new therapeutic and diagnostic technology using PI polyamide and nanostructure in neuroblastoma

Syouta UEKUSA, Tsugumichi KOSHINAGA
Medical Group

Beckwith-Wiedemann syndrome (BWS) is a genomic imprinting disorder in human with a variable phenotype. The major features are anterior abdominal wall defects involving exomphalos (omphalocele), pre- and postnatal overgrowth, and macroglossia. Additional less frequent complications include specific developmental defects and a predisposition to embryonal tumours. BWS is associated with genetic or epigenetic alterations in one of two imprinted domains on chromosome 11p15.5. The most frequent alteration associated with BWS is the absence of methylation at the maternal allele of KvDMR1, an intronic CpG island within the *LIT1* gene. It has been suggested that KvDMR1 locus is an imprinting control region (ICR) that regulates multiple genes in 11p15.5. In this domain, *LIT1* regulates the expression of imprinted genes in *cis*. One of the anti-tumor genes p57KIP2 is located in the 11p15.5 region. Reduced or loss of p57KIP2 expression seems to cause of high incidence of embryonal tumors and we hypothesized that down-regulation of *LIT1* expression could result in up-regulation of p57KIP2 and reduction of cell growth.

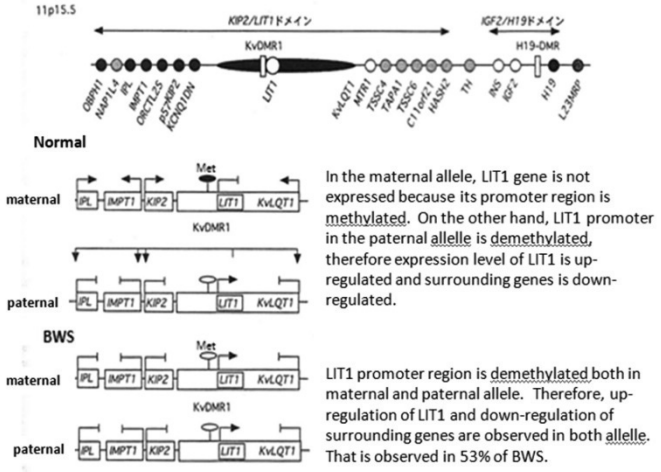

PI polyamide can recognized DNA and bind to it in a sequence specific manner. PI polyamide designed to recognize a transcription factor binding site could inhibit transcription factor to bind to its target site and down-regulate expression of target gene. In the present study, we designed the PI polyamide for the promoter region of *LIT1* gene, and examined whether the LIT1 PI polyamide can reduce the expression level of *LIT1* ,up-regulate p57KIP2 expression and show anti-cancer effect in BWS fibroblast cell lines.

In vitro experiments

We designed PI polyamide targeting for CAAT box, which is located on promoter region of *LIT1* (h-CCAAT1, h-CCAAT3). BWS fibroblast cell lines (BWS6, 9) were cultured in the presence or absence of PI polyamide, h-CCAAT1, h-CCAAT3, for 72hours. Expression of p57KIP2 was highly up-regulated in the cells treated with PI polyamide compared with the cells cultured without PI polyamide treatment.

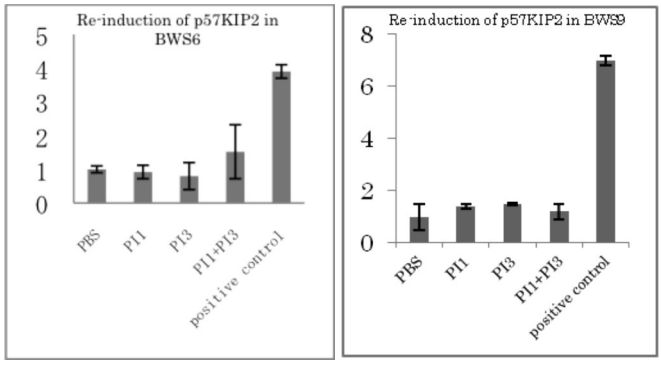

Since it was confirmed that the PI polyamide targeting promoter region of *LIT1* have the effect to down-regulate p57KIP2 expression, we are now testing the effect of the PI polyamide on nephroblastoma cell lines and examining whether the PI polyamide can up-regulate the expression level of p57KIP2 and show anti-tumor effects.

Experimental Studies for Quantum Memory using Neutral Atoms

Takeshi KUWAMOTO
Quantum Information Group

Quantum memory is a key element in quantum information and computing technology. Our purpose in this project is realizing the quantum memory using neutral atoms. We especially aim at the long-term storage of quantum entangled states in the atomic system.

1. Quantum light source

- Increase in intensity of orthogonally polarized photon pairs resonant with a transition in rubidium atom -

In order to gain the strength of 795-nm-wavelength orthogonally polarized photon pairs, which are used for generating the quantum entangled states in the future, we reinforced the output power of a 397.5-nm-wavelength light source used for generating the 795-nm photon pairs through spontaneous parametric down conversion process.

The 397.5-nm light was obtained by second harmonic generation (SHG) with a type I PPKTP crystal. We developed a bow-tie-type cavity for boosting the SH light (397.5 nm) power. As a result, the SH light power and the number of orthogonally polarized photon pairs increased about threefold.

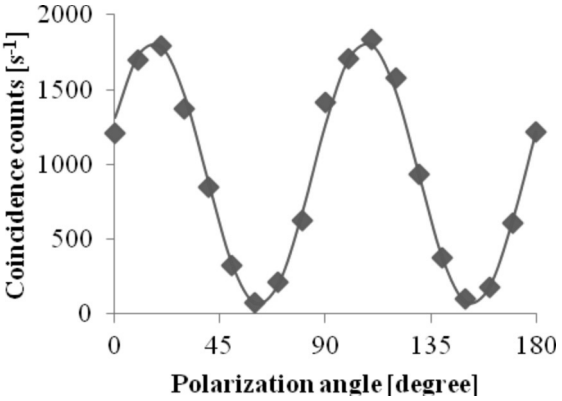

We measured the two-photon interference of the generated orthogonally polarized photons (figure on the right). The obtained visibility was 93%, and the result states that the generated photon pairs have clear quantum nature.

The next step is storing the orthogonally polarized photons in the Rb atoms.

2. Light storage system

- Improvement in efficiency of light storage in Rb atoms using electromagnetically induced transparency -

Last year we develop an optical-phase & frequency-lock loop (OPFLL) system in order to lengthen the storage time of light in atoms. Although the storage time increased twofold, the improvement in storage efficiency was not observed. So, we developed the high-speed injection-current controller of the laser, which functioned by receiving the feedback signal from the OPFLL. In addition, a hot-water temperature control system for Rb cell was introduced to reduce magnetic field around the cell.

Figure on the right shows the experimental results measured before (red) and after (blue) the improvements (storage time is 5 ms). The storage efficiency of light was increased twofold.

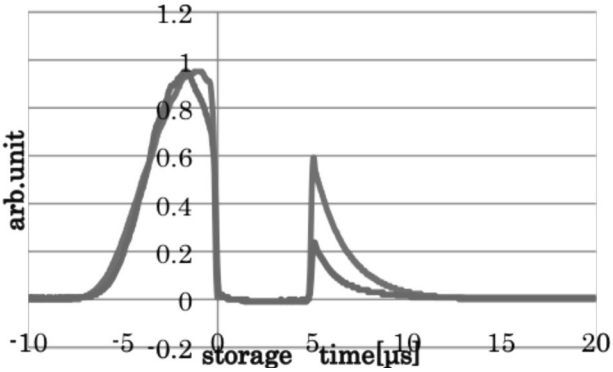

Application to the iPS induced factors of DP-1 Stabilon motif inhibiting proteolysis

Yoshikazu MASUHIRO
Medical Group

Induced pluripotent stem cells are cells developed in Japan and have possibility to become the cell source of the regenerative medicine in the future. However, quality control of iPS is important so that induced pluripotent stem cells are really applied to regenerative medicine. In this study, I try construction of the iPS-producing method using the proteins as a method without gene variation. In this study, I examine the iPS-producing method establishment using proteolysis resistant cell-permeable proteins and only reagents by the cooperation with the researchers of the N. research project, because the old method using the cell-permeable proteins is complicated, and the production efficiency is low.

1. Application to the iPS induced factor of the DP-1 Stabilon motif

Transcription factors (Oct4, Sox2, Klf4, cMyc) called the Yamanaka factors are necessary to derive induced pluripotent stem cells. However, when we use cMyc, it is reported that a ratio to produce a cancer in iPS transplant mouse. Recently, it was reported that the transcription factor called Glis1 facilitated the iPS production efficiency even if cMyc was not used. Therefore we thought about the production of genetically safe iPS with the cell membrane permeable protein of Oct4, Sox2, Klf4 and Glis1.

In addition, I discovered the DP-1 Stabilon motif which raised stabilization of the protein in a conventional study in this laboratory (article 2). It fused in an N- or C-terminus of Yamanaka4 factor and Glis1, and investigated this Stabilon whether stabilization of these protein was possible. As a result, when I transfected these factors expression plasmid into HEK 293 cells and transiently expressed, and analyzed expression by Western blotting, Stabilon-fused Glis1, Oct4, Sox2 and Klf4 were stabilized. The effectiveness varied according to molecular species by an N- or C-terminal fusion.

2. Function elucidation of the proteolysis-resistant mechanism of the DP-1 Stabilon motif

The mechanism is unknown why DP-1 Stabilon enables stabilization of the protein. I speculate that mechanisms of protein stabilization by Stabilom is the resistance of proteolysis, translation efficiency or localization. Many molecules which were selectively functioned by Stabilon were known that degraded by ubiquitin-proteasome system. Therefore I examined whether Stabilon maintained proteolysis resistance of the protein by pulse chase assay using the cycloheximide. As a result, absence of Stabilon, the expression level of protein rapidly attenuated. But the presence of Stabilon, the expression level of protein slowly attenuated. Therefore, a function of Stabilon was more likely to be proteolytic resistance. Next, I examined a ubiquitinyation of Stabilon fusion proteins, it was at the same level in having Stabilon or not. Then, I examined resistance for the proteasomal proteolysis by an in vitro proteasomal assay. As a result, the proteins completely disintegrated without Stabilon in six hours, but Stabilon fused proteins were hardly degraded. Therefore, it was considered that the function of Stabilon was resistance for proteasomal proteolysis. Next, I examined the resistance for various protease. As a result, Stabilon maintained resistance for the chymotrypsin-like serine protease. Because proteasome have caspase-like, trypsin-like, chymotrypsin-like activity, it is considered that the function of Stabilon is resistance for chymotrypsin-like activity of proteasome. Others, it is considered that the influence of interaction between Stabilon fused protein and proteasome, or unfold, this mechanism is examined in detail now.

Pharmacokinetic/Pharmacodynamic Analysis of Tumor-localizing Photosensitizing Compounds

Takahiko AOYAMA, Yoshiaki MATSUMOTO
Medical Group

To describe the relationships between effects following photodynamic therapy, light dose, and plasma compound concentration, we develop a high-performance liquid chromatography (HPLC) method for the determination of plasma concentration and investigate the pharmacokinetics of novel compound CT101019a (Fig. 1).

Pharmacokinetics of CT101019a

A simple and sensitive HPLC method is developed for the determination of plasma CT101019a concentration in rats and apply to the pharmacokinetic study. Separation was achieved on a reversed-phase TSK-GEL ODS-80 column by gradient elution using sodium phosphate solution (pH 2.7) and acetonitrile. The flow rate was 1.3 ml/min. The elute was monitored by a fluorescence detector with respective excitation and emission wavelengths of 412 and 644 nm. The method was used to determine the plasma concentration time profiles of CT101019a after intravenous injection. The observed plasma concentration time profiles of CT101019a and talaporfin (Fig. 2) are shown in Fig. 3. The half-life of CT101019a was shorter than that of talaporfin. These characteristics of CT1101019a are suitable for clinical application.

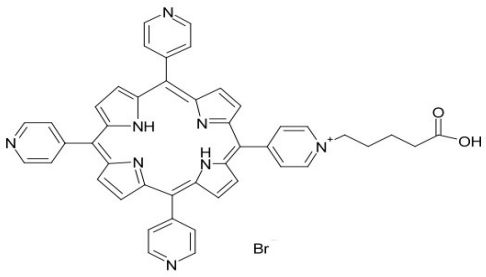

Fig. 1. Chemical structure of CT101019a.

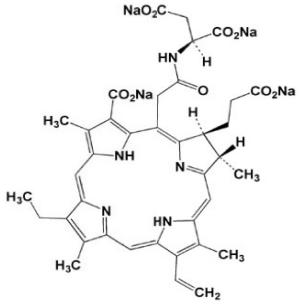

Fig. 2 Chemical structure of talaporfin sodium.

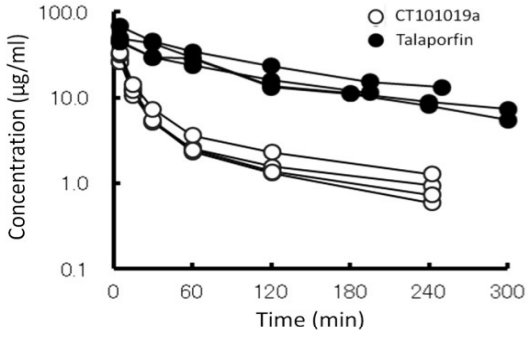

Fig. 3. Plasma concentration-time curves.

Self-assembly and Self-organization from the viewpoint of Device-fabrication Methods

Sachiko MATSUSHITA
Supramolecular and Self-Assembly Group; Energy Technology Group

Two subjects related with self-assembly and self-organization were studied with perspective of the developments of unexplored scientific fields and new technology: 1) Dye-sensitized photonic crystal electrodes, and 2) Fabrication of optical devices via self-assembly.

1. Dye-sensitized photonic crystal electrodes

The combination of dye-sensitized solar cells and photonic crystals is actively studied. We had reported the improvement of the photoelectric conversion efficiency of dye-sensitized solar cells combined with a self-assembled-type photonic crystal, i.e., TiO_2 inverse opal. However, whether these results were caused by the photonic crystal effect or the nano/mesoscopic effect was unclear. The major reason is the luck of full-photonic band-gap (FPBG) structure composed of TiO_2 and electrolyte. The authors had discovered such FPBG structure by computer simulation.

This time, we demonstrated the high aspect ratio microfabrication process of (001)TiO_2 for photoniccrystal structure by SF_6-RIE technique to prepare the FPBG structure. Cr micro patterns as an etching mask material were prepared on a TiO_2 single crystal (rutile) by photolithography and radio frequency (RF) sputtering. The TiO_2 was anisotropically etched along [001] by optimizing the etching conditions. The higher selectivity etching rate ratio of TiO_2/Cr was obtained by lower RF power and higher flow rate of SF_6. In addition, higher anisotropic etching with a higher aspect ratio was achieved by higher RF power and high flow rate of SF_6. This project is collaboration with Dr. H. Hashiba at Department of Engineering and Science.

2. Fabrication of optical devices via self-assembly

Noble metal nanoparticles or nanostructures display localized surface plasmon resonances (LSPRs) depends on geometry. In terms of using such nanostructures in optical nanodevices, the planar and symmetric arrangement of tips on a particle is highly advantageous in controlling the polarization property and handling the particle. Here we report an inexpensive process for preparing a six-rayed star-like nanostructure using a self-assembly technique that satisfies above features and is suitable for use in optical nanodevices. The method is based on a combination of colloidal self-assembly, thermal sintering and chemical etching of SiO_2 particles, which together enable the tuning of both the size of the particles and neck diameter. A six-rayed star-like nanostructure was formed in the above procedure (Figure, inset). The absorption peaks red-shifted with an increase in the Au coating time (Figure). The simulated coating thickness of Au is also shown on the top x-axis in the Figure. The difference between the peak shift caused by Au thickness and the peak shift by the nanostructure is observed. When the coating time was less than 20 s, the absorption peaks of the 2D colloidal crystal and the six-rayed star-like nanostructure were observed at a shorter wavelength than those of the substrate. These blue shifts might have been caused by sharpness at the tip and tiny spaces among particles. For a coating time of 30 s, the absorption peaks of the nanostructure and the substrate were observed at the same wavelength. This result revealed that the tip sharpness on the nanostructure was abated in the thicker Au film.

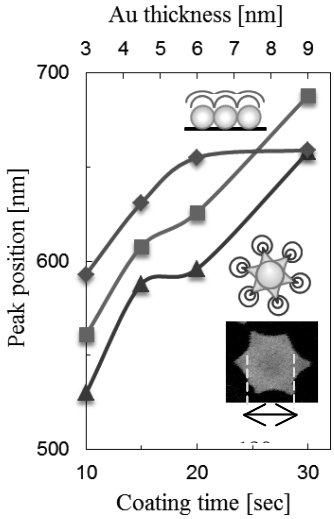

Figure. UV–Vis spectrum change of substrate (♦), 2D colloidal crystal (■), and six-rayed star-like nanostructure (▲) with Au coating time. The SEM image of six-rayed star-like nanostructure is shown in the inset.

Applied chemical biology: strategy to cure cancer patients

Hiroki NAGASE
Medical Group

Exploiting an enormous amount of potentials of organic chemistry, we have conducted chemical biological approaches to cure cancer patients. Following two distinct but important approaches have been studied for the last four years and promising progresses have been made. The first one is DNA binding molecule of PI polyamide for cancer therapy and the second is a novel chemosensitizing radiation therapy.

1. PI polyamides targeting cancer related genes for anti-cancer therapy

Pyrrole-Imidazole (PI) polyamide molecule was originally designed from structures of natural DNA binding molecule, such as Distamicine and Diocarbamicine and has been discovered as a synthetic molecule which recognizes the minor groove of Watson-Click base pair of double-stranded DNA in a sequence-dependent manner. We have developed a semi-automatic synthesis system for PI polyamide, which are able to regulate specific target gene-expression under specific transcription factor binding inhibition for biological functional studies and perhaps patient therapy. PI polyamide immediately penetrated the nucleus *in vitro* and *in vivo* without any vehicle. After intra venous injection it rapidly reduce the serum concentration, delivered to most of tissue cells, excreted to urine or bile juice and did not metabolize in animals. The PI polyamides, designed for anti-Tgfb1 and anti-MMP9 activity, were well tolerated, reduced target gene expression and showed therapeutic effects in animal models of human diseases. For instance, after I.V. administration of anti-MMP9 polyamides, tumor metastasis was significantly suppressed in the mouse model of human liver metastasis of colon cancer. This new auto-synthetic chemicals can be designed for many transcriptional regulation of transcripts and applied to prove many biological hypothesis of transcriptional regulation for cancer research, and may be used for cancer therapy in the future.

2. A novel chemosensitizing radiation therapy by using synthetic porphyrin derivatives

Photodynamic therapy (PDT) is a medical treatment that uses a photosensitizing chemical and a light source (long wave length light can reach around 1cm depth of human tissues) to activate the applied chemical. The result is an activated oxygen molecule that can destroy nearby cells. Precancerous cells and certain types of cancer cells can be treated by PDT. Cancer cells uptake more of the porphyrin derivatives and retain the chemicals in a long duration. Thus, the PDT can introduce a cancer cell specific therapy. We invented the radiation-sensitizing chemical of the porphyrin derivatives, which can be used for PDT and may also induce photon activation therapy (PAT), provoking the emission of Auger electrons after inducing a photoelectric effect. X-ray radiation allows for the treatment of cancers that are deep inside the human body. We observed an induced cancer cell death after irradiation following administration of the porphyrin derivative. This study orchestrated harmony of works among medical school, school of pharmacy and college of science and technology.

Research for high density and high speed magnetic recording
- Thermally assisted magnetic recording applying near field optical light -

Katsuji NAKAGAWA
Information Storage Group

It is a challenging issue to write magnetic domains on a stable magnetic recording layer for the future high density magnetic recording technology, because the stable magnetic recording layer for high density recording is extremely sustainable not only against thermal agitation but also against recording magnetic field. We study thermally assisted magnetic recording that can enable to write nano-meter size magnetic domains on stable magnetic film by the technique that applies the confined laser light by a near field optical method. The structure of surface plasmon antennas is designed by optical and thermal simulation collaborated. Magnetic films and fabrication e-beam lithography processes for surface plasmon antenna are also prepared. We have also started femto-second laser pulse recording collaborated with Assistant Prof. A. Tsukamoto and Prof. A. Itoh.

1. Design of Near-Field Surface Plasmon Antenna

We studied optical intensity and temperature distribution after femto-second laser pulse irradiation for the structure model as shown in Fig. 1. The direction of irradiated optical electric field is adjusted to the surface plasmon antenna in parallel to the Au antenna. The peak intensity which is enhanced by the surface plasmon effect is observed at the edge of the antenna, but the peak temperature at the edge becomes broad by the effect of thermal diffusion. The ratio between the first peak and the second peak of temperature depending on time after light irradiation is shown in Fig. 2. It was found that the first peak temperature is much higher than the second peak in 10 ps after the laser irradiation.

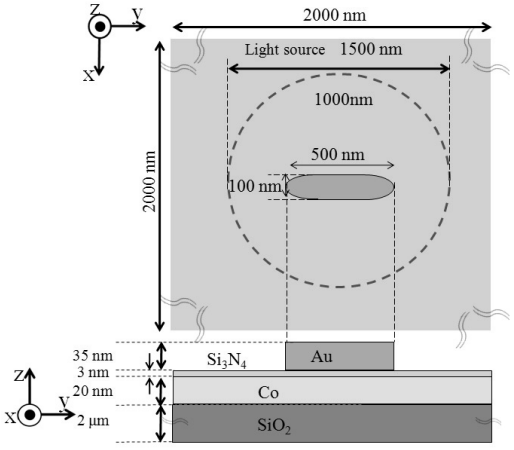

図１　プラズモンアンテナ構造例

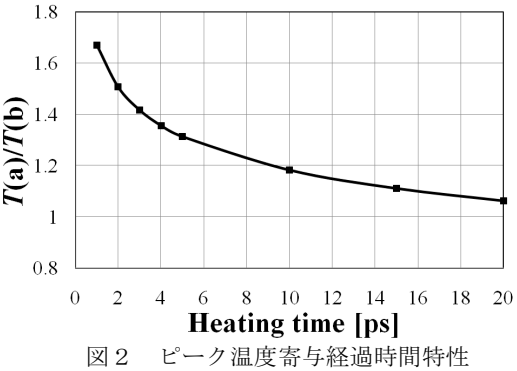

図２　ピーク温度寄与経過時間特性

2. Recording Film and Antenna Fabrication

CoCrPt alloy magnetic film was prepared as a recording film by sputtering method. E-beam lithography was applied to fabricate Au surface plasmon antenna. A block made of one hundred Au antennas in 50 by 50 micron square can be made on the magnetic film. A few blocks of Au antennas were fabricated on the film for femto- second laser recording test.

3. Coupling between Surface Plasmon Antenna and Wavegude

It is very important how to locate surface plasmon antennas in magnetic head for thermally assisted magnetic recording. We studied the dependence on energy transfer efficiency to get high efficiency. One of the methods that surface plasmon antennas are placed along with a waveguide was investigated by simulation. The method can be applied for creating a confined circularly pola

Composite Formation of Hydrogen Occlusion Alloys and Photo-Related Phenomena Thereof

Nobuyuki NISHIMIYA
Energy Technology Group

Novel methods for converting photo-energy to hydrogen energy have been developed through combination of hydrogen-absorbing sites with natural or artificial centers where photo-assisted hydrogen dissociation takes place.

1. Highly efficient photo-chemical energy conversion by combination of photo-water splitting systems with encapsulated hydrogen absorbing alloys

Bacteria with photosynthetic activity to split water on irradiation was chosen as a system for water splitting, ZrVFe alloy encapsulated with tetraethoxysilane-silicone rubber precursor was chosen as an encapsulated hydrogen absorbing alloy, and the combination of the bacteria and the alloy proved to be highly efficient in water splitting to shift the equilibrium to the hydrogen evolution side. The encapsulated ZeVFe alloy that was able to absorb and recover bio-hydrogen repeatedly occluded hydrogen from hydrogen-oxygen mixtures with molar ratio of hydrogen to oxygen of 2 as illustrated in Fig. 1. Hydrogen was released at elevated temperatures after occlusion of the mixtures. ZrVFe that was not encapsulated could once absorb hydrogen, but got inactive in the following runs.

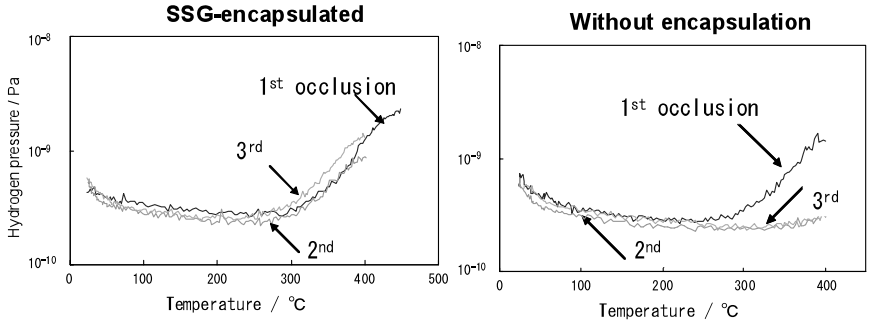

Fig. 1 Hydrogen Evolution in vacuo after hydrogenation under hydrogen-oxygen mixture with hydrogen to oxygen ratio of 2 at room temperature.

The scope of hydrogen absorbing materials was further spread to CVD (Chemical Vapor Deposition) single walled carbon nanotubes, novel B-C-N compounds etc. beyond the conventional metallic alloys.

2. Hydrogen battery chargeable by photon energy through combination of hydrogen absorbing alloys and photo-active systems that create electron-hole pairs on irradiation

Occluded hydrogen was stabilized in $ZrMn_2$, Ti-Zr-Fe-Mn alloys etc. when irradiated at 352 nm in vacuo in the presence of a photocatalyst WO_3. It was confirmed from higher temperature shift of hydrogen desorption in temperature programmed desorption analyses. Occlusion of hydrogen under a hydrogen atmosphere and stabilization of occluded hydrogen would provide with photo-assisted charging of secondary batteries.

3. Hydrogen occlusion with varied stability by hydrogen absorbing alloys assisted by photocatalysts that dissociate hydrogen

Photo-assisted hydrogen desorption was observed for a complex hydride $LiBH_4$ in the presence of WO_3 and a co-catalyst CuO. Hydrogen in the complex hydride was destabilized on irradiation and the temperature for hydrogen desorption was lowered. Such was also the case for $NaBH_4$ and $Mg(BH_4)_2$. The stability of hydrogen in a typical non-metallic material, C-N, was also

Nano-Electromagnetic Simulation and Its Applications to Plasmonic Devices

Shinichiro OHNUKI
Quantum Theory and Computation Group

This work aims at developing fast and reliable electromagnetic simulation methods for studying the interaction between light and nanoscale objects. We apply our computational methods to designing nanoscale devices, such as plasmonic antennas and single-molecule rotors, through the collaboration with researchers of the *N.* research project.

1. Plasmonic Antennas with Particulate Media for All Optical Magnetic Recording

The arrangement of particulate media under the nano-scale plasmonic antenna has been investigated. Figure 1 shows the structure of a plasmonic antenna to enhance the intensity of the electric field inside the center particle. When the liner polarized light impinges, the localized circular polarized light is produced in the center particle and the intensity becomes double compared with adjacent particles.

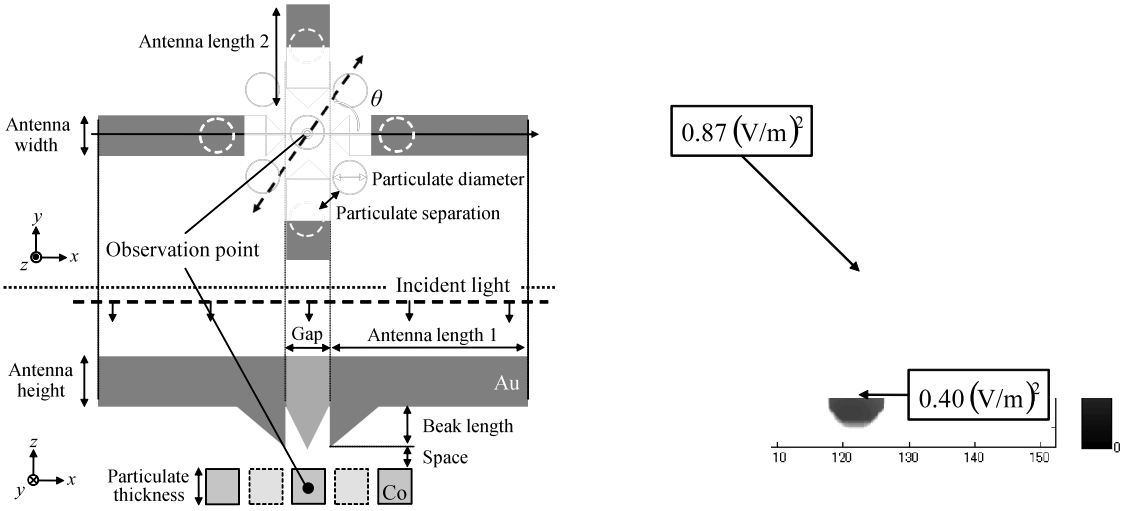

Figure 1: Plasmonic antenna with particulate media

2. Time Domain Solvers Based on Integral Equation Methods

We have developed fast and accurate solvers based on integral equation methods with fast inverse Laplace transform for time domain electromagnetic problems. Applying the multilevel fast multipole method, the computational time is about five times faster. Our method is suitable for parallel computing and the efficiency keeps almost 100 % for increasing the number of nodes. We are investigating nano-aperture antennas and charge distribution on a nano-particle due to an electric dipole source.

3. Coupled Solver of Maxwell and Schrödinger Equations

A novel algorithm is proposed for solving coupled Maxwell and Schrödinger equations relying on the use of a length gauge form of the coupling between an electromagnetic field and electrons. The proposed algorithm can reduce computational time almost by half as compared with the conventional method.

4. High-Precision Analysis of Electromagnetic Scattering Problems

A point matching method can analyze electromagnetic scattering problems with a high degree of accuracy. We study computational accuracy of the electromagnetic scattering from homogeneous dielectric spheres. Compared with the analytical solutions, our error control is verified.

Self-Assembled Supramolecules and Their Applications to Energy, Medical, and Information Technologies

Joe OTSUKI
Supramolecular and Self-Assembly Group; Energy Technology Group

Self-assembly of appropriately designed molecules will afford a bottom-up method for producing nanostructures. This work aims at developing new molecular self-assembling systems, revealing self-assembled structures and dynamic behaviors at the molecular level, and searching for applications of self-assembly to energy, medical, and information technologies through the collaboration with researchers of the *N*. research project.

1. Structures and dynamic behaviors of molecular self-assemblies at the molecular level

Self-assembly of new double-decker complexes, in which two disk-like moieties, such as porphyrin and phthalocyanine, sandwich a metal ion, has been investigated. We provide evidence that a heteroleptic double-decker complex of cerium with phthalocyanine and porphyrin ligands undergoes rotational libration in solution for the first time on the basis of variable-temperature ^{1}H NMR. On the other hand, the zirconium complex with the same set of ligands undergoes no rotational motion. These molecules deposited on graphite surfaces exhibited different shapes in scanning tunneling microscope (STM) images, revealing difference in the rotational motion at the molecular level. (*Chem. Lett*. 2011, Figure).

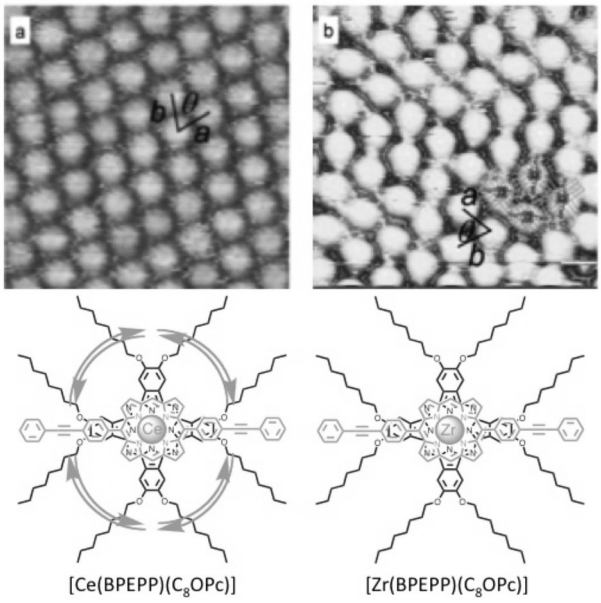

We have also reported the assembling behaviors of a double-decker porphyrin complex appended with an additional porphyrin group with submolecular resolution (*J. Nanosci. Nanotechnol*., in press).

2. Piperidine-Substituted Perylene Sensitizer for Dye-Sensitized Solar Cells

We have prepared perylene sensitizers and studied the photovoltaic performance in dye-sensitized solar cells (DSSCs) (*Adv. OptElectr.* 2011). Physical properties and photovoltaic performance of this new perylene derivatives have been reported. A piperidine-substituted perylene dye, when anchored to nanocrystalline TiO_2 films, achieves very efficient sensitization across the whole visible range extending up to 800 nm. Under standard AM 1.5 irradiation (100 mW cm^{-2}) and using an electrolyte consisting of 0.6 M dimethylpropylimidazolium iodide, 0.05M I_2, 0.1 M LiI, and 0.5 M *tert*-butylpyridine in acetonitrile, a solar cell containing the sensitizer yielded a short-circuit photocurrent density of 7.7 mA cm^{-2}, an open-circuit photovoltage of 0.57 V, and a fill factor of 0.70, corresponding to an overall conversion efficiency of 3.1%.

3. Preparation of compounds for the X-ray based photodynamic therapy

Photodynamic therapy (PDT) is one of the cancer treatment methods that destroys cancer cells using dyes and laser irradiation. The problem in this method is that visible-light laser used in the treatment cannot penetrate into the body more than 1 cm in depth. In an attempt to combine X-ray irradiation and PDT, we are searching for porphyrin derivatives which are effective under X-ray irradiation. We have so far found two effective compounds at the cell experiment level.

Conjugate-Fermi-hole analysis in the origin of Hund's rule and the interaction between atoms and strong ultrashort pulsed laser lights

Tokuei SAKO
Quantum Theory & Computation Group

On the basis of the recently proposed new concept of "conjugate Fermi holes" the origin of Hund's rule in simple atoms has been analyzed and clarified by the structure of the internal wave functions. Ionization of these atoms as a fundamental process of the light-matter interaction has been also studied by focusing on the non-perturbative ionization of He by EUV-FEL lights, which was reported recently at Spting8. A theoretical model explaining the observed trends has been constructed.

1. Conjugate Fermi holes and Hund's multiplicity rule in He-like atomic systems

The origin of Hund's multiplicity rule in the low-lying excited states of the helium atom has been studied by considering the two-dimensional helium atom. The internal part of the full configuration interaction wave functions for the (2s) and (2p) singlet-triplet pairs of states has been extracted and visualized in the three-dimensional internal space (r_1, r_2, ϕ_-). The internal wave function of the singlet states without electron repulsion has a significant probability around the origin of the internal space while the corresponding probability of the triplet wave function is negligible in this region due to the presence of a Fermi hole. The electron-electron repulsion potential has been visualized also in the internal space. It manifests itself by three striking poles penetrating exactly into the spatial region defined by the Fermi hole. Because of the existence of these strong potential poles in the vicinity of the Fermi hole a major part of the singlet probability migrates out of this region. In contrast, the corresponding triplet wave function is less affected by these poles due to the presence of the Fermi hole. The singlet probability is shown to migrate from its original region close to the origin to a region far away where either r_1 or r_2 are large. This results in a more diffuse electron density distribution and a smaller electron repulsion energy of the singlet state than of the corresponding triplet state. The mechanism of the evolution of the singlet probability toward the region of large r_i (i =1, 2) in the presence of the electron repulsion potential has been rationalized on the basis of a new concept called conjugate Fermi hole.

2. Non-perturbative resonance ionization of He by high-intensity and high-frequency laser lights

Two-photon resonance ionization probability of atoms in strong extreme-ultraviolet free-electron laser (EUV-FEL) pulses has been investigated by the model of the time-dependent wave packet propagation of a light-coupled multi-level atom. Under the simulation within the model assuming single mode FEL pulses, the ionization probability P_{ion} has shown characteristic dependences on the scaled coupling-parameter U_{gi} between two levels of the ground (g) and intermediate resonance (i) states, namely, $P_{ion} \propto (U_{gi})^n$ with n being equal to ~2, less than 1, and ~1 for the small, medium, and large U_{gi} regimes, respectively. This power dependence of the ionization probability has been interpreted due to Rabi oscillations between g and i states. To compare with recent experimental results on the same condition, the multi-mode nature of SASE-FEL pulses has been managed in the simulation. Then, the recent experimental laser-power dependence of the two-photon resonance ionization of He [Sato *et al*., J. Phys. B **44**, 161001 (2011)] has been well described by that for the large U_{gi} regime of the simulation, i.e., n ~1. Thus, the observed linear laser-power dependence has been rationalized as being caused by the strong Rabi oscillations between the ($2p$) – ($1s$) states.

Synthesis of Nano-rod Devices with Wide Band Gap Semiconductor Effect

Kaoru SUZUKI
Nanomaterials and Nanodevices Group

My research aims at fabrication of nano-materials and nano-devices for high functional applications such as nano-tube sensor, nano-rod transistor and wide band gap semiconductor nano-film for water-splitting by using fundamental techniques of nano-process and fabrication of nano-materials. Using the achievement of the investigation, progress of energy conversion system, information technology and biotechnology can be expected.

1. Metal encapsulated carbon nanotube for magnetic force microscope probes

We have synthesized directly ferromagnetic metal (Ni, Fe, Co) and antiferromagnetic maetal (Cu) encapsulated carbon nanotubes (CNTs) for probe of magnetic force microscope on a mesh grid for viewing transmission electron microscope (TEM) by pyrolysis of ethanol solution. These metals inside CNTs identified Ni, Fe, and Co with energy dispersive X-ray (EDX) spectrum analysis. The diameter and length of the metal core is in the range of 10 – 80 nm and 100 – 800 nm with varying heating period and temperature, respectively. The walls consist of cylindrical graphene sheets with 3 -50 layer. The diameter of metal core possesses inclinable to enlarge at other temperature between 1013K and 1123K.

2. Synthesize of Photocatalytic $Sr_xLa_{1-x}TiO_3$ Film for Hydrogen Generation with Visible Area in Solar Light Excitation by Laser Induced Forward Transfer Method

La doped TiO_2 have attracted great interest for photocatalytic properties, which can be used visible area in solar light although only TiO_2 limiting with ultra violet area. However, these reports were almost powdered $La_2Ti_2O_{7.}$ To circumvent this problem, we have attempted to synthesized La doped TiO_2 thin film on polymer films substrate by laser induced forward transfer method. In addition we have tried to Sr doped as imparity for improvement photocatalystic effect. These films were composed of several molar ratios. We have successfully crystallized perovskite structure films which were La doped TiO_2 thin film of $La_2Ti_2O_{7,}$ Sr doped TiO_2 thin film of $SrTiO_3$ and both impurity doped thin film of $Sr_xLa_{1-x}TiO_3$ (x=0.1~0.9). The best of photocatalystic effect was realized by $Sr_{0.7}La_{0.3}TiO_3$ to $SrTiO_3$, and furthermore, the band gap of $Sr_{0.3}La_{0.3}TiO_3$ was 3.2 eV which showed the same tendency. As a result, the molar ratio of $Sr_{0.7}La_{0.3}TiO_3$ thin film confirmed suitable to hydrogen generation.

3. Synthesis of (SrLaF)FeAs superconducting thin films by the photo excited pulsed laser deposition

The synthesis of the high T_c superconducting thin films is very important for the electronic device use. Among Fe-based superconductors, a Co-doped $SrFe_2As_2$ epitaxial film is reported to become a superconductor with T_c of 20 K. However, in order to obtain superconducting films by pulsed laser deposition (PLD), there are some problems such as expensive substrates and high quality target materials. The photo excited PLD (PE-PLD) is considered to have advantages for the synthesis of high quality epitaxial thin films. (SrLaF)FeAs is isostructural to (LaO)FeP and $(Sr_{0.6}La_{0.4}F)FeAs$ becomes superconducting below T_c of 26.3 K. In this study, we have tried to prepare superconducting (SrLaF)FeAs thin films by PE-PLD, and investigated the relation between the wavelength of the photo excitation sources and the crystallization of films. They are deposited on MgO (001) substrates by PLD using a Nd:YAG laser (wavelength: 532 nm, fluence: 1.5 J/cm^2) with the photo excitation. The photo excitation sources are IR (from 0.5 to 2.5 μm), Xe (from 0.2 to 1.1 μm) and LED (peak: 400 nm, width: ± 20 nm). While X-ray diffraction patterns of (SrLaF)FeAs thin films excited by IR or normal PLD show only impurity phases, those excited by Xe or LED show some oriented peaks of (SrLaF)FeAs. This result indicates that the excitation by ultra violet rays increases a reaction ability and has an effective role of the growth of the superconducting epitaxial films.

Mechanism of Superconductivity in Layered Fe-based Superconductors and Search of New Superconducting Compounds

Yoshiki TAKANO
Nanomaterials and Nanodevices Group

Since the discovery of superconductivity at 26 K in $LaFeAsO_{1-x}F_x$, many researches on the iron-based superconductors have been carried out and the new superconducting compounds with the parent phases of SrFeAsF are found. It is reported that the superconducting transition temperature T_c of $Sr_{0.6}La_{0.4}FeAsF$ is 26 K and that of $Sr_{0.5}Sm_{0.5}FeAsF$ is 56 K. However, as the study of $Sr_{1-x}R_xFeAsF$ besides R = La and Sm is quite a few, superconducting properties of them have not been clarified now. In 2010, oxygen deficient $LaFeAsO_{0.89}$ is also reported to be a superconductor with T_c of 28 K. On the other hand, we have studied the electrical and magnetic properties of LaZnPnO (Pn=P, As, Sb) before the discovery of iron based superconductors. Recently, it is reported that the optimum value of y which shows the highest T_c varies with x in $LaFe_{1-y}Zn_yAsO_{1-x}F_x$.

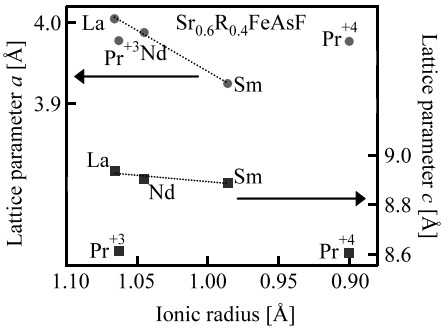

Fig. 1 R dependence of lattice parameters.

1. Crystal Structure and Superconducting Properties of $Sr_{1-x}R_xFeAsF$ (R=La, Pr, Nd, Sm)

We have succeeded to prepare $Sr_{1-x}R_xFeAsF$ (R=La, Pr, Nd, Sm) although a small amount of SrF_2 impurity is observed. Figure 1 shows the R dependence of the lattice parameters for $Sr_{1-x}R_xFeAsF$ with x=0.4. Lattice parameters for R=Pr are quite different from those for other rare earths. This implies that Pr ions are not trivalent in $Sr_{1-x}R_xFeAsF$. The superconducting transition temperature for R=Pr are also different from those for other rare earths (Fig. 2).

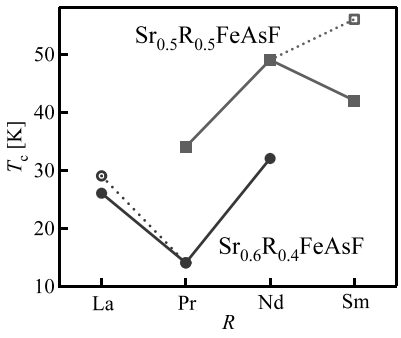

Fig. 2 R dependence of superconducting transition temperature. Open symbols are reported values.

2. Preparation and Electrical Properties of $SrFeAsF_{1-x}$

We have prepared almost single phase samples of $SrFeAsF_{1-x}$. The defficiency of F in F sites are confirmed from the increase of the relative intensity of (111) reflection in X-ray diffraction patterns. The temperatrure dependence of the electrical resistivity is analyzed by the following formula; $r(T)=r_0+AT^n$ (Fig. 3). Although superconductivity is observed in the samples with n =1~2 for other iron based superconductors, it is not observed in the sample with x = 0.25 which has n of 1.08 in this system.

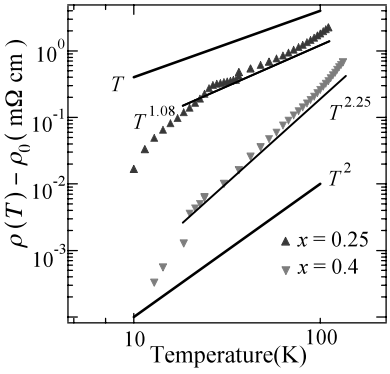

Fig. 3 Relation between log(r (*T*)- r $_0$) and log*T*.

2. Crystal Structure and Electrical Properties of $LaFe_{1-y}Zn_yAsO$

We have tried to prepare $LaFe_{1-y}Zn_yAsO$ for $0 \le y \le 1$. Mixed phase samples with LaFeAsO and LaZnAsO are obtained for middle region of y. Almost single phase samples are obtained for $y \le 0.2$. Lattice constants a and c increases with y in this region.

Ultra Fast Information Recording and Ultra Fast Photo Magnetic Switching

Arata TSUKAMOTO, Akiyoshi ITOH
Information Storage Group and Supramolecules and Self-Assembly Group

The ever increasing the capacity of storing information motivates the search for faster approaches to process and magnetically record information. Most computers store data on magnetic hard disk drives, in which the direction – "up" or "down" – of the magnetic moments in a small region of the disk corresponds to a binary bit. However, it was faced to unavoidable fundamental problem for faster operation in conventional way known as ferromagnetic resonance limit. We have experimentally demonstrated controlled magnetization reversal induced by a single 40 femtosecond (40 x 10^{-15}s) circularly polarized laser pulse in the magnetic GdFeCo thin film, a material relevant for data storage. This finding, previously believed to be fundamentally impossible, reveals an ultrafast and efficient pathway for writing magnetic bits. Based on deep understanding of relationship between light and magnet including above new discovery, we are striving to establish the fundamental techniques of researching and developing ultrafast spin manipulation.

1. Film structure dependence of demagnetization time scale of GdFeCo metallic thin films

In conventional magneto-optical (MO) recording which triggered with nanoseconds pulsed laser irradiation, the time scale of heat-up and cool-down process depends on thermal diffusion property in multilayered recording media. The speed limits of heating and cooling process are important issue for fast heat assisted magnetic recording. Femtosecond pulsed laser light allow excitation of magnetic systems much shorter than the time scale of thermal diffusion. In this study, we investigated the film structure dependence of ultrashort laser-induced demagnetization of 20 nm thick GdFeCo alloy films, under the variety of with / without intermediate dielectric layer and heat sink layer. After the laser excitation, we found two time region from magnetic behavior: rapid step-like reducing process of magnetization and following recovering process with precessional motion. Figure 1 shows the ultrafast magnetic response of 20 nm thick GdFeCo alloy films triggered with ultrashort laser pulse irradiation measured by all-optical pump-probe method. Simultaneously, change of normalized reflectivity *DR* / *R* was measured for monitoring the time evolution of electron temperature.

The time scale of first rapid step-like demagnetization processes is conformed as within picoseconds range independently with film structure, which is much shorter than characteristic time scale of ferromagnetic resonance for all the cases. Following hundreds ps regime, film structure dependent precessional motion of magnetization was appeared. (Publication 7)

2. Development of measurement system

We set up the system applying a fine adjustment manipulator. Laser pumping and probing system can be precisely adjusted by the new motorized system.

A new magnetic bias coil was prepared for applying up to 1 kOe. The bias field can be synchronized to the laser system.

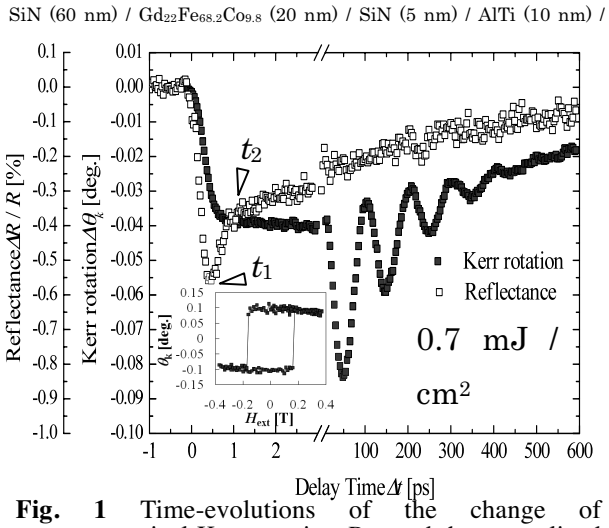

Fig. 1 Time-evolutions of the change of magneto-optical Kerr rotation Dq_k and the normalized change of reflectivity *DR* / *R* of 20nm thick $Gd_{22}Fe_{68.2}Co_{9.8}$ alloy films. Inset figures show the magneto- optical Kerr effect hysteresis loops of each sample measured by same time-resolved observation set-up without pump laser.

Propagation Characteristics and Distribution of Energy Flow by Dielectric Waveguide with Diamond Dielectric Structure in the Middle Layer

Tsuneki YAMASAKI
Quantum Theory and Computation Group

In periodic structures such as photonic crystal structures, it is known that a frequency stop band occurs. Consequently, in the design of photonic crystal structures with periodic constants same as optical wavelength, it is important to investigate the stop band region. On the one hand, it can be controlled optical constants by the development of manufacturing technology of semiconductor and optical devices. Thus, many analytical and numerical techniques have been proposed that are applicable to dielectric gratings having arbitrary structures. To deal with multilayered dielectric circular cylinder arrays such as photonic crystal structure, it is necessary to analyze the multilayered periodic arrays. In the multilayer method, as the inhomogeneous region is divided into an assembly of stratified thin layers with step index profile, the matrix size depends on the number of layers. In our method, the order of characteristic matrix equation depends on the modal truncation number, but it does not depend on the number of layers.

In recent paper, we analyzed the guiding problem for the dielectric waveguides composed of dielectric circular cylinders and loaded with diamond dielectric structure in the middle layer, and investigated the propagation characteristics by using a combination of improved Fourier series expansion method and multilayer method.

Numerical results are given by complex propagation constants in the first stop band region and distribution of energy flow at the guided region for both TE_0 and TM_0 modes. It is shown inFig.1 and Fig.2 that a diamond is the best structure for storing electromagnetic energy for both TE_0 and TM_0 modes compared with triangular structure.

These results have been 「Reference」 as follows:

Reference：

(1)R. Ozaki and T. Yamasaki: “Propagation Characteristics of Dielectric Waveguides with Arbitrary Inhomogeneous Media along the Middle Layer”, IEICE Trans. Electron. vol.E95-C, no.1(2012).

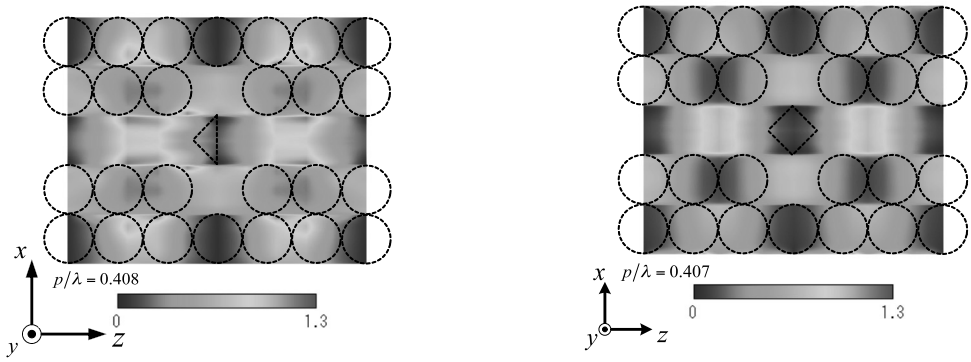

(a) Triangular structure (b)Diamond structure

Fig.1 Distribution of energy flow for the case of TE mode for $\varepsilon_3^{(m)}/\varepsilon_0 = 3$.

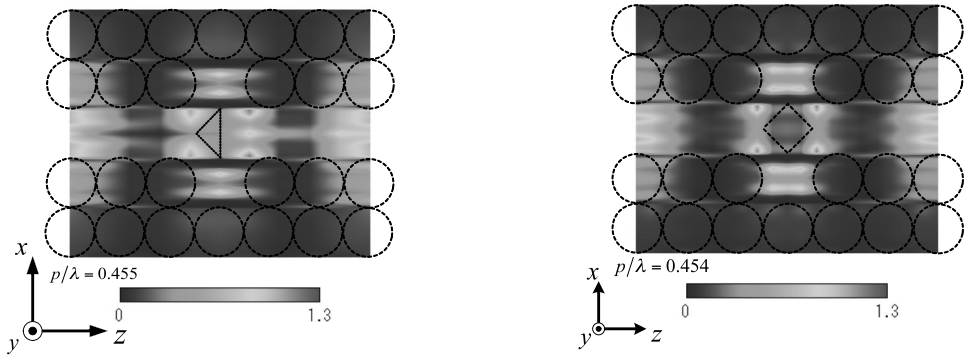

(a) Triangular structure (b)Diamond structure

Fig.2 Distribution of energy flow for the case of TM mode for $\varepsilon_3^{(m)}/\varepsilon_0 = 3$.